

New geochemical and palaeontological data from the Permian-Triassic boundary in the South African Karoo Basin test the synchronicity of terrestrial and marine extinctions

Jennifer Botha, Adam K. Huttenlocker, Roger M.H. Smith, Rose Prevec, Pia Viglietti, Sean P. Modesto

PII: S0031-0182(19)30728-X

DOI: <https://doi.org/10.1016/j.palaeo.2019.109467>

Reference: PALAEO 109467

To appear in: *Palaeogeography, Palaeoclimatology, Palaeoecology*

Received date: 4 August 2019

Revised date: 11 November 2019

Accepted date: 14 November 2019

Please cite this article as: J. Botha, A.K. Huttenlocker, R.M.H. Smith, et al., New geochemical and palaeontological data from the Permian-Triassic boundary in the South African Karoo Basin test the synchronicity of terrestrial and marine extinctions, *Palaeogeography, Palaeoclimatology, Palaeoecology* (2018), <https://doi.org/10.1016/j.palaeo.2019.109467>

This is a PDF file of an article that has undergone enhancements after acceptance, such as the addition of a cover page and metadata, and formatting for readability, but it is not yet the definitive version of record. This version will undergo additional copyediting, typesetting and review before it is published in its final form, but we are providing this version to give early visibility of the article. Please note that, during the production process, errors may be discovered which could affect the content, and all legal disclaimers that apply to the journal pertain.

New geochemical and palaeontological data from the Permian-Triassic boundary in the South African Karoo Basin test the synchronicity of terrestrial and marine extinctions

Jennifer Botha<sup>1, 2</sup>, Adam K. Huttenlocker<sup>3</sup>, Roger M. H. Smith<sup>4, 5</sup>, Rose Prevec<sup>6, 7</sup>, Pia Viglietti<sup>8</sup> and Sean P. Modesto<sup>9</sup>

<sup>1</sup>National Museum, PO Box 266, Bloemfontein, 9300, South Africa

<sup>2</sup>Department of Zoology and Entomology, University of the Free State, Bloemfontein, 9300, South Africa, jbotha@nasmus.co.za

<sup>3</sup>Department of Integrative Anatomical Sciences, University of Southern California, Los Angeles, CA 90033, USA, ahuttenlocker@gmail.com

<sup>4</sup>Evolutionary Studies Institute, University of the Witwatersrand, Johannesburg, 2050 South Africa, Roger.Smith4@wits.ac.za

<sup>5</sup>Karoo Palaeontology, Iziko South African Museum, Cape Town, 8000, South Africa

<sup>6</sup>Department of Earth Sciences, Albany Museum, Makhanda, 6139, South Africa, r.prevec@am.org.za

<sup>7</sup>Department of Botany, Rhodes University, Makhanda, 6140, South Africa

<sup>8</sup>Integrative Research Center, Field Museum of Natural History, 1400 South Lake Shore Drive, Chicago, IL, 60605, United States, pviglietti@fieldmuseum.org

<sup>9</sup>Department of Biology, Cape Breton University, Sydney, NS, Canada, sean\_modesto@cbu.ca

Keywords: End-Permian; Early Triassic; Mass Extinction; Gondwana

## Abstract

The end-Permian mass extinction (EPME) is widely recognized as the largest mass extinction in Phanerozoic history. In marine strata the main extinction event is well constrained, and has been radiometrically-dated to an interval of some 60 kyr, approximately 251.9 million years ago. However, the age and duration of the EPME in the terrestrial realm, as well as its possible synchronicity with that of the marine realm, is debated. Here, we shed light on issues pertaining to the identification and position of the terrestrial EPME in southern Africa. Using recently collected sedimentological (facies sequences), palaeontological (biostratigraphic ranges), geochemical (stable isotope analyses) and detrital zircon (ID-TIMS) data from a new site in the Xhariep District of the South African Karoo Basin, we demonstrate that the Permian-Triassic boundary sequence containing evidence for phased tetrapod extinctions is time equivalent with the marine extinction. We conclude that the terrestrial EPME recorded in the Karoo may be regarded as essentially synchronous with the EPME currently defined in the marine realm, and was likely the result of the same volcanically-induced atmospheric disturbances. This study describes the first single, vertical succession of vertebrate and plant fossils that span the terrestrial Permian-Triassic boundary that are also well-constrained both by relative (stable isotopes) and absolute (detrital zircon geochronology) dating methods.

## 1. Introduction

### 1.1 The end-Permian mass extinction

The end-Permian mass extinction (EPME) was the most devastating ecological crisis in Phanerozoic history. Its effect on both marine and terrestrial ecosystems substantially changed community structure causing a severe reduction in global biodiversity (Xie et al., 2005; Yin et al., 2007; Chen et al., 2009; Shen et al., 2011; Smith and Botha-Brink 2014). Recent geochronological evidence constrains the event to between  $251.941 \pm 0.037$  and  $251.880 \pm 0.031$  million years ago (Ma) using U-Pb dated zircons from ash beds sampled in the marine Global Boundary Stratotype Section and Point (GSSP) at Meishan, South China (Burgess et al., 2014). Although many causes for the extinction have been proposed, there is broad consensus that ecosystem collapse was catalyzed by emission of greenhouse gases during prolonged volcanic eruption and subsequent sill intrusions in northern Pangaea, as evidenced by the extensive Siberian Traps flood basalts (Renne et al., 1995; Payne and Kump, 2007; Grasby et al., 2011; Black et al., 2012; Burgess et al., 2017). The proposed effects of this volcanogenic gas and dust pollution on the marine realm include benthic acidification, anoxia, hypercapnia, euxinia, and excessive methane release from deep sea gas hydrates, leading to a rapid decline in biodiversity (Alroy, 2008; Wignall et al., 2010; Brennecka et al., 2011; Loope and Kump, 2013; Foster and Twitchett, 2014; Lau et al., 2016). In the continental realm in Gondwana, increasingly warmer and drier climatic conditions along with considerably less reliable rainfall triggered a similar large-magnitude reduction in primary productivity and terrestrial biodiversity in general (Smith and Botha-Brink, 2014; Rey et al., 2016; MacLeod et al., 2017). These conditions have been argued to have resulted in unstable communities and heightened extinction risks for the survivors for at

least five million years after the event, based on trophic network models (Roopnarine et al., 2007, 2019; Roopnarine and Angielczyk, 2015).

### *1.2 Rationale for the present study*

South Africa's Karoo Basin has provided the most complete record of the effect of the terrestrial EPME, and numerous field investigations have yielded precise biostratigraphic records of Karoo tetrapods throughout the uppermost Permian to lowermost Triassic (e.g. Smith, 1995; Smith and Ward, 2001; Hancox et al., 2002; Retallack et al., 2003; Smith and Botha, 2005; Botha and Smith, 2006; Smith and Botha-Brink, 2014; Viglietti et al., 2018a). By integrating sedimentological, biostratigraphic, palaeomagnetic and geochemical data, these studies have led to the identification of a relatively continuous PTB interval in the Karoo Basin. The interval is characterised by a basin-wide sequence of sedimentary facies associations that indicate progressive lowering of regional groundwater, increased seasonality, and climate drying (Smith and Botha-Brink, 2014; MacLeod et al., 2017; Viglietti et al., 2018a).

The PTB sequence coincides with a three-phased extinction of tetrapods and the apparent disappearance of glossopterid-dominated floras (Smith and Botha Brink, 2014). Within the lower Palingkloof Member, an interval of laminated reddish-brown and olive-grey siltstone-mudstone couplets has been used as a marker for the main extinction pulse. This is associated with the basin-wide last appearance of the Permian dicynodonts *Daptocephalus leoniceps*, *Dicynodontoides recurvidens*, *Dinanomodon rubidgei* and *Lystrosaurus maccaigi*. The overlying massive siltstone facies of the upper Palingkloof Member marks the first appearance of the archosauriform *Proterosuchus fergusi*, *Lystrosaurus declivis* and *L. murrayi* (Smith and Botha-Brink, 2014). This sequence records substantial turnover and alterations to community structure and resilience (Roopnarine and Angielczyk, 2012, 2015,

2016; Roopnarine et al., 2007, 2019), while also preserving the distinctive geochemical signatures of the PTB. The latter include a negative  $\delta^{13}\text{C}$  excursion (MacLeod et al., 2000; Ward et al., 2005) in addition to other chemostratigraphic and radiometric age constraints (Coney et al., 2007).

Nevertheless, a few recent studies have disputed the placement of the biostratigraphically-defined PTB in South Africa (Steiner et al., 2003, Gastaldo et al., 2009, 2015, 2019), calling into question the synchronicity of intrabasinal faunal turnover (Gastaldo et al., 2015), as well as the evidence for basin-wide aridification in the earliest Triassic (Tabor et al., 2007, Gastaldo et al., 2014, 2017). Consequently, these studies have catalyzed a reinvestigation of the timing of the main extinction event and its correlation to that of the marine realm (Gastaldo et al., 2015), an effort that has been aided by new geochronologic age constraints including radiometric dates presented here by our team. Here, we present new sedimentological, biostratigraphic, and geochemical data, including radiometric dates from detrital zircons, collected from a recently recognised terrestrial PTB site in the main Karoo Basin. Our multidisciplinary study evaluated the accuracy of the widely accepted position of the EPME in the main Karoo Basin, and contributes to the debate about its synchronicity with the marine EPME.

## 2. Historical context

Until the turn of the century, most research on the EPME focused on marine strata (Jin et al., 2000), whereas complete terrestrial Permian-Triassic boundary (PTB) sequences were considered to be rare or absent within continental basins. More recently, however, relatively continuous terrestrial PTB sections have been investigated in South Africa, Russia, Antarctica, Australia and China, allowing researchers to examine the timing and mechanisms

of terrestrial extinctions using multi-proxy approaches (e.g. Ward et al., 2000; Smith and Ward, 2001; Benton et al., 2004; Retallack et al., 2005; Collinson et al., 2006; Metcalfe et al., 2009, 2015; Cui et al., 2017; Fielding et al., 2019). Consequently, several techniques have been used to identify sedimentological and geochemical signatures of the mass extinction, in addition to the floral and faunal turnovers that are apparent across the PTB. Sedimentological studies have revealed changes in fluvial style and modification of floodplain environments across the PTB in Antarctica (Webb and Fielding, 1993; Collinson et al., 2006), South Africa (Smith, 1995; Ward et al., 2000; Smith and Botha-Brink, 2014), Spain (Arche and López-Gómez, 2005), Russia (Newell et al., 1999), China (Metcalfe et al., 2009; Yang et al., 2010; Zhang et al., 2016) and some parts of Australia (Retallack et al., 1998; Michaelsen, 2002; but see Fielding et al., 2019). These generally manifest as a change from high-sinuosity, meandering river systems with expansive, wet floodplains through a straightening transition stage to low-sinuosity, braided ephemeral river channels with seasonally dry floodplains subject to flash floods (Ward et al., 2000; Smith and Botha-Brink, 2014).

Associated with these large-scale environmental changes, a distinctive chemostratigraphic signature, represented by a steep negative  $\delta^{13}\text{C}$  excursion at the PTB, has been observed at sites in South Africa (MacLeod et al., 2000, 2017; Ward et al., 2005; Coney et al., 2007), Antarctica (Retallack et al., 2005) and China (Cao et al., 2008; Thomas et al., 2011; Cui et al., 2017), mirroring that preserved in marine sediments (Korte and Kozur, 2010). Investigations of  $\delta^{13}\text{C}$  excursions in combination with precise zircon ages from multiple ash beds at the GSSP at Meishan have allowed precise dating of this geochemical signature (Shen et al., 2011, 2012, 2013), tying it to similar chemostratigraphic records in the terrestrial Karoo Basin of South Africa (MacLeod et al., 2000; Ward et al., 2005; Coney et al., 2007) as well as to the famous Siberian Traps (Burgess et al., 2014, 2017). Ongoing studies have shown that excursions recorded in terrestrial sediments, such as those in the

Permo-Triassic Palingkloof Member (Balfour Formation) of the Karoo Basin, mark the beginning of a series of  $\delta^{13}\text{C}$  excursions that occurred throughout much of the Early Triassic. Importantly, they provide evidence for prolonged carbon cycle fluctuations indicating extreme climate perturbations and environmental stress (Retallack et al. 2005, Payne et al., 2004; Payne and Kump, 2007; Clarkson et al., 2013; Sanson-Barrera et al., 2015).

Although the magnitude and timing of resulting extinctions has been studied extensively in marine sections (Erwin et al., 2002; Foster and Twitchett, 2014; Zaton et al., 2016), the extent and rate of biodiversity loss in the terrestrial realm are still debated. Terrestrial vertebrate fossil assemblages spanning the PTB reveal a complex scenario of extinctions and reduced diversity in some clades, and increased abundance and diversity in others (Benton et al., 2004; Irmis and Whiteside, 2011; Irmis et al., 2013; Fröbisch, 2013; Smith and Botha-Brink, 2014). For example, temnospondyl amphibians, procolophonid parareptiles, archosauromorph reptiles and cynodont therapsids continued to diversify after the extinction event (in the Induan stage), becoming key players in Triassic ecosystems (Ruta and Benton, 2008; Nesbitt et al., 2013; Ruta et al., 2013a; MacDougall et al., 2019). By contrast, pareiasaurian parareptiles and gorgonopsian therapsids disappeared completely, while the surviving therocephalian and dicynodont therapsids persisted with reduced diversity and low rates of cladogenesis despite fairly strong abundances (Ruta et al., 2013b; Huttenlocker et al., 2011; Huttenlocker, 2014; Smith and Botha-Brink, 2014). Most notable among these is the disaster taxon *Lystrosaurus*, the most common tetrapod found in the earliest Triassic of the Karoo Basin, South Africa, but also known from Triassic beds on multiple continents such as the marine-to-terrestrial Panchet beds of India where its connection to the marine Triassic was first established (Tripathi and Puri, 1961, 1962). With the exceptions of *L. maccaigi* and *L. curvatus*, which have both been found in the latest Permian, the other species of South African *Lystrosaurus* are exclusively Triassic in age.

(Botha and Smith, 2006, 2007; Smith and Botha-Brink, 2014). As in therapsids and cynodonts (Huttenlocker, 2013; Huttenlocker and Botha-Brink, 2013, 2014), histologic and taphonomic evidence show that Early Triassic *Lystrosaurus* exemplified a general pattern of elevated early mortality and attenuated growth typical of most post-extinction therapsids (Viglietti et al., 2013; Botha-Brink et al., 2016).

The effects of end-Permian extinctions on plants remain poorly understood. At a very coarse resolution, the changes in Gondwanan floras from the late Permian to the Middle Triassic are profound, where the distinctive *Glossopteris*-dominated forests of the Permian gave way to the much more diverse gymnosperm floras of the Middle-to-Late Triassic typified by the peltasperm *Dicroidium* (Anderson and Anderson, 1985; Retallack, 2005, 2013; Anderson et al., 2007; Lindström and McLoughlin, 2007). Some studies of macrofloral and particularly palynological evidence indicate that the global PTB turnover was more of a transition than a mass die-off (Gastaldo et al., 2005; Lindström and McLoughlin, 2007; Saxena et al., 2018; Fielding et al., 2019) or even that, at the generic level, the floras of the world were minimally affected (Nowak et al., 2019). Fielding et al. (2019) even noted that the terrestrial turnover in Australia was asynchronous with the marine extinction. Additionally, as more localities are studied it appears that key index taxa such as *Glossopteris* and *Dicroidium* had overlapping ranges in some regions (Kerp et al., 2006; Saxena et al., 2018). However, other authors have maintained that gymnosperm-dominated late Permian floral communities experienced a devastating crisis during the EPME (McElwain and Punyasena, 2007; Cascales-Miñana and Cleal, 2014; Yu et al., 2015; Cascales-Miñana et al., 2016), and were in some regions succeeded by pioneering fern and lycopsid floras that persisted into the early Middle Triassic (Retallack, 1995; Wang, 1996; Looy et al., 2001; Grauvogel-Stamm and Ash, 2005). As suggested by Rees (2002), it is likely that plant communities showed different patterns of extinction and recovery in different parts of the

world, and in the absence of high resolution studies of the changes in macrofloras across the PTB, the pace and nature of this transition continues to be a source of debate (eg. Fielding et al., 2019; Nowak et al., 2019). One of the greatest challenges facing palaeobotanists is the rarity of earliest Triassic plant fossils (Gastaldo et al., 2005; Nowak et al., 2019). Increasing global temperatures at the close of the Permian and into the Triassic, and the postulated increase in aridification and seasonality (with accompanying fluctuations in water table) in the interior regions of Pangaea, may provide a taphonomic explanation for this rarity. These conditions would have decreased the preservation potential of fossil plants regionally and the likelihood of encountering those rare habitats that favoured plant preservation (Gastaldo, 2005). These effects are certainly apparent in the Karoo Basin, where there is generally a decline in plant fossil abundance and quality in the late Changhsingian, with the first well-preserved floras and coal seams above the PTB only reappearing in the lower parts of the Upper Triassic (Anderson and Anderson, 1985; Anderson et al., 2007; Gastaldo et al., 2005). While the fossil macrofloras of the upper Permian and Middle Triassic clearly represent highly disparate plant communities, the pace and nature of the changes that took place over this interval remain poorly understood within the context of the Karoo Basin. Only through continued and concerted efforts to find the sparse macroplant fossil evidence in the uppermost Permian and lowermost Triassic strata, at multiple sites across the basin, will progress be made towards reconstructing the floral changes that occurred in concert with the patterns of extinction seen in the vertebrate faunas.

### **3. Study site and techniques**

#### *3.1. Field techniques*

The field site extends over three adjoining farms (Nooitgedacht 68 [site locality 30°19'37.49"S 25°55'57.99"E], Vogelstruis-fontein 69, now called Droogefontein 176 [site locality 30°20'22.08"S 25°55'45.39"E], and Geluksfontein 204 [site locality 30°20'28.03"S 25°55'46.7"E]) approximately 20 km north of the town Bethulie in the Xhariep Municipal District (previously Bethulie District), Free State Province, South Africa (Fig. 1A, B). Previously, Botha-Brink et al. (2014) described the sedimentary sequence and palaeontology of PTB exposures on the farm Nooitgedacht 68, reporting a diverse assemblage dominated by the end-Permian synapsid *Lystrosaurus maccaigi*. A subset of these specimens is presented in Table 1. The current study area includes two neighboring localities, namely an isolated flat-topped butte called ‘Loskop,’ and a pinnacle and adjacent ridge called ‘Spitskop’ approximately 800 m southwest of Loskop (Fig. 1C, D). Loskop is on the farm Nooitgedacht 68, whereas Spitskop extends over Nooitgedacht 68, Vogelstruis-fontein 69 and Geluksfontein 204 (Fig. 1B). Both localities contain an apparently complete sequence of uppermost Permian and lowermost Triassic strata preserving the terrestrial PTB and its associated faunal turnover from the upper *Daptocephalus* to lower *Lystrosaurus* assemblage zones (Fig. 2).

Initial stratigraphic logging by Botha-Brink et al. (2014) suggested that the two prominences are equivalent in age, based on their lateral continuity over a short distance, apparently continuous sedimentation, and similar vertical changes in the faunal assemblages at both localities. In this study, a new stratigraphic section totaling 122 m was logged on Spitskop from its lowermost exposures in the Balfour Formation to its summit in the middle Katberg Formation. The logs were measured using standard field techniques, using a Jacob’s staff and Abney level, to an accuracy of 10 cm. The lithology, rock colour (using Munsell geological rock colour-chart 2009 revision), sedimentary structures, bedding planes, scour surfaces, nodules, root traces, fossils and burrows were recorded onto each log (Fig. 3, Table

1, Supplementary Fig. S1, Supplementary Table S1). A list of in situ fossil taxa incorporating all of the Bethulie (northern basin) and Graaff Reinet (southern basin) study sites to date is presented in Supplementary Table S2.

### *3.2. Stable isotope geochemistry*

In-situ carbonate nodules collected from Permian and Triassic palaeosols on both Loskop (17 horizons) and Spitskop (12 horizons), were consumptively sampled for carbon and oxygen stable isotope analysis (Fig. 3). Nodules were impact fractured and fresh surfaces milled for rock powder. Septarian nodules with visible crystalline structure in hand samples were excluded from the analysis. Diagenetic calcite veins were also sampled where possible to control for diagenetic signatures. At least one nodule from each palaeosol profile was milled, although multiple nodules were sampled closer to the palaeontologically-defined EPME in order to identify potential variability in the isotopic signatures. Enamel samples were also taken from Permian theriodont therapsid teeth in order to compare their carbon and oxygen isotope signatures with those of the pedogenic nodules.

Micritic or finely-crystalline nodules and enamel samples were milled into a fine powder using a Dremel tool with diamond-tipped bit, deposited onto a wax paper sheet, and poured into small microcentrifuge tubes. For the theriodont enamel samples, only about one milligram of sample was taken from two positions on either the mesial or lingual surfaces of the teeth. Both basal and apical enamel samples were taken to account for variations in isotopic signatures of individual teeth during their biomineralization.

Analyses were performed at the University of Utah, Salt Lake City, USA. The sample powders were weighed into silver capsules (approximately 50–100 micrograms of powder per capsule) and dried under a vacuum at a temperature of 200°C approximately two hours before analysis. The samples were analysed for  $\delta^{13}\text{C}$  and  $\delta^{18}\text{O}$  on a Finnigan MAT 252

coupled to a Carboflo dual-inlet carbonate device. The stable isotope ratios are reported as  $\delta$  values relative to the international standard Vienna Pee Dee Belemnite (V-PDB), using the standard per mil (‰) notation. SD of an internal carbonate standard was  $\pm 0.1\text{ ‰}$ . For each microcentrifuge tube of enamel powder, approximately 400 micrograms of sample were weighed into silver capsules to ensure sufficient yield, and the above steps were followed using an internal enamel standard. Carbonate standards used included Carrara Marble and LCVEC lithium carbonate. Enamel standards included FGS (fossil gomphothere) and FRS (fossil rhino). All standards have been calibrated to NBS 19.

### *3.3 Detrital zircon U-Pb radiometric dating*

A sandstone bed bearing volcaniclastics in the lower portion of the Spitskop section—approximately 6.5 m below the palaeontologically-defined EPME and within facies B (lower Palingkloof Member) (Fig. 3)—was identified during our 2015 collecting trip and was found to contain a high yield of detrital zircons. Hand samples were collected from unweathered rock, stored in clean, plastic collecting bags, and transported to the laboratory where zircons were isolated using standard separation techniques. The samples yielded approximately 3.3 zircon crystals per cc. Up to 80 crystals were picked at random and mounted in epoxy, polished, and imaged using SEM cathodoluminescence to visualize internal zoning and to select ablation spots.

We first assessed age probabilities of zircon populations using laser ablation inductively coupled plasma mass spectrometry (LA-ICPMS), and then estimated maximum depositional age of the youngest zircons using high-precision isotope dilution thermal ionization mass spectrometry (ID-TIMS). Determination of age probabilities was first conducted at the University of Utah LA-ICPMS laboratory, although age profiles from additional beds were also assessed at the Central Analytical Facilities of Stellenbosch

University for comparison, following a subsequent collecting trip in 2017 (Supplementary Information). Of the LA-ICPMS sample from facies B, 15 crystals from among the youngest population were selected and analyzed at the Berkeley Geochronology Center using ID-TIMS. Prior to ID-TIMS, the sample was abraded chemically and thermally annealed to remove zones of potential Pb loss.

## 4. Results

### *4.1. Palaeoenvironmental interpretation and biostratigraphy of the PTB facies sequence*

Despite slight differences in thickness, the sequence of sedimentary facies across the PTB on both Loskop and Spitskop is the same (A–E in Figs. 1C, D and 3A, B) and similar to that described by Smith and Botha-Brink (2014) from the farm Bethel 763 (a.k.a, “Bethal”) some 35 km southeast of the study site. From the lowest (A) to the highest (E) the sequence is as follows:

#### *4.1.1. Facies A—Massive greyish-brown mudrock*

This facies (Fig. 3, Table 1, Supplementary Fig. S1, Table S1) comprises stacked 1 m-thick tabular beds of blocky-weathering structureless greyish-brown (2.5Y/2) mudstone, and rare erosional-based, fine-grained sandstone bodies. The latter are generally light grey (5Y7/1) on Loskop and more olive-grey (5Y4//2) on Spitskop. The sandstones range from 1–5 m thick and are structured by massive bedding at the base, grading and fining upwards into ripple cross-laminated fine-grained sandstone stringers with irregular, low-angle (10–15°) erosive bases that have previously been interpreted as lateral accretion units (Smith, 1987). The massive greyish-brown muddy siltstone commonly hosts laterally continuous 1 m-thick

horizons containing scattered oblate smooth-surfaced brown-weathering nodules. The nodules range from 5–20 cm in diameter and internally they commonly display small brecciated mudrock clasts floating within a grey micritic siltstone matrix.

The interpreted depositional setting for the massive greyish-brown mudrock facies is an expansive, generally dry, but seasonally wet, floodplain between meanderbelt ridges comprising multi-lateral sand-dominated point bars (Jackson, 1981; Labrecque et al., 2011). Floodwaters periodically overtopped, and in places broke through, the leveed channel banks, inundating the floodplain. In the proximal floodplain areas the floods deposited thin layers of silt that were generally readily incorporated into the soil A horizon. However, some flood events resulted in much thicker deposits that effectively killed the soil profile and simultaneously raised the water table. These events are preserved in the section as mottled massive siltstones with horizons of oblate smooth-surfaced carbonate nodules containing brecciated mudrock, which are interpreted as having been precipitated subsurface in pond margin environments on generally wet floodplains that are subjected to seasonal drying (Alonso-Zarza, 2003). Near the base of the section (+/-1.5 m on Fig. 3A) a conspicuous horizon of vertically and horizontally-oriented calcareous rhizocretions is evidence of fluctuating water tables in a lower part of a calcic palaeosol (Klappa, 1980). In summary, we interpret the pedogenic mottling of the massive grey mudrock facies as evidence of gleyed alluvium affected by a high watertable for most of the year with a short, warmer, dry season. Within the seasonally fluctuating vadose zone of the floodplain alluvium, calcite was precipitated around roots and clots of decaying plant matter resulting in the horizons of carbonate rhizocretions and nodules.

An impression of a large tree branch was found approximately 24 m below the PTB on Loskop (Fig. 3A; figured in Botha-Brink et al., 2014). Dicynodont therapsids identified as *Daptocephalus leoniceps* (Fig. 5A) and *Lystrosaurus maccaigi*, which are index species of

the upper Permian *Dapocephalus* Assemblage Zone (AZ) (previously *Dicynodon* AZ see Viglietti et al., 2016), were recovered from facies A around the base of Loskop and Spitskop. Botha-Brink et al. (2014) previously assigned several dicynodont specimens to *Dicynodon lacerticeps* based on the absence of nasal bosses and the presence of a narrow intertemporal region and tusks, but the last two features apply to *Dapocephalus leoniceps* as well. Viglietti et al. (2016) re-examined the stratigraphic placement of dicynodont specimens re-identified in a recent study by Kammerer et al. (2011) and found that none of the *Dicynodon* specimens were from the uppermost part of the biozone. As only *Dapocephalus* was found to extend to the upper boundary of the zone, Viglietti et al. (2016) renamed the biozone the *Dapocephalus* AZ. The specimens from Loskop and Spitskop were re-examined and reassigned to *Dapocephalus leoniceps* based on the presence of a long, narrow, straight (in dorsal view) intertemporal bar and tusks that are at the level of the anterior margin of the orbits and the newly constrained biostratigraphy (Kammerer et al., 2011; Viglietti et al., 2016; Kammerer 2019).

The presence of theriodonts such as a new species of gorgonopsian (based on Botha-Brink et al., 2014) and the therocephalians *Ictidosuchoides longiceps* and *Moschorhinus kitchingi* confirm that the lower slopes represent the upper *Dapocephalus* AZ (Botha-Brink et al., 2014).

#### 4.1.2. Facies B—Massive mottled dark reddish-brown / olive-grey mudrock

This facies (Fig. 3, Table 1, Supplementary Fig. S1, Supplementary Table S1) on Loskop and Spitskop comprises vertically stacked 0.25–5 m-thick tabular beds of mottled dark reddish-brown (2.5YR 2.5/4) and olive-grey mudstone with light grey (on Loskop) or olive-grey (on Spitskop) siltstones with interbedded thin (<0.5m) lenticular siltstone and fine-grained sandstone bodies displaying distinctively “gullied” basal contacts and climbing ripple

cross-stratification indicative of rapid scour-and-fill sedimentation. The degree of mottling varies, but notably irregularly-shaped dusky-red (5Y4/2) mottles appear within this facies. The mottled mudstones contain claystone-lined root moulds and horizons of brown-weathering calcareous nodules some of which contain fossil bone. Of possible regional significance is a horizon of large “stellate” nodular masses that occur in the upper part of this facies on both sections (23.5 m on Spitskop log and 14.5 m on Loskop log of fig 3, Supplementary Fig. S3A). Each nodular mass comprises 3–5 radially-arranged fissures that taper outwards from a central cavity and are filled with vertically-orientated calcareous laminae. In cliff outcrops these large (+/- 0.5 m diameter) nodules are evenly-spaced along strike approximately 10 m apart. They are interpreted to be part of a large scale polygonal network of shrinkage cracks possibly related to drying of the alluvium on the ancient floodplain as regional water tables dropped (Khadkikar et al., 1998; Smith and Botha, 2005). We begin to observe at both Spitskop and Loskop, distinctive tubular *Katbergia* burrow casts in this facies (Supplementary Fig. S3B). These 2–3 cm diameter, straight, cylindrical burrow casts dip at a consistent 45°, but are randomly oriented. They display a knobbly outer surface with many small ridges mostly at a low angle to the long axis of the cast, that have been interpreted as grooves in the tunnel walls made by a scratch-digging decapod (Gastaldo and Rolerson, 2008).

The sandstone bodies are composed of two to three vertically-stacked units structured by horizontal lamination that grades upwards into climbing ripple cross-lamination. A few of the elongated basal scours contain lenses of reworked mudrock pebbles and flakes, but pedogenic glaebules are rare.

This facies marks the first appearances of patchy reddening in the mudrocks along with vertically stacked sheet sandstones with fluted and gullied basal surfaces, and *Katbergia* burrows. The onset of mudrock reddening in the upper Balfour Formation has been

previously recognized as a feature marking the base of the Palingkloof Member (Johnson, 1976). We also find increased maturity of the palaeo-pedogenic carbonate horizons, xeromorphic taproot structures and changes in the taphonomic style of the tetrapod fossils in this facies. Smith and Botha-Brink (2014) noted that the majority of the in situ tetrapod fossils recovered from this facies comprised partial rather than complete bones with evidence of pre-burial breakage and the preferential preservation of maxillary caniniform processes, basioccipitals and isolated cervical vertebrae of both *Moschorhinus kitchingi* and *L. maccaigi*. Although colour alone does not indicate increased aridity (Li et al., 2017), we consider the combination of the features listed above to be linked to a lowering of the watertable in the floodplains along with a change from seasonally fluctuating yet still perennial flow to more ephemeral flash flood-type hydrology in the distributary channels (Smith and Botha-Brink, 2014). This interpretation is supported by recent isotopic studies that have found climatic changes such as increased aridity in the upper *Daptocephalus* Assemblage Zone (MacLeod et al., 2017; Rey et al., 2016, 2017).

Plant fossils were found in the uppermost Permian facies (Fig.4A–F) on both Spitskop and Loskop. Sphenophyte axes with longitudinal ribbing continuous through the nodes are common in both facies A and B. *Paracalamites* stems preserve well in the fossil record and are one of the few types of plant remains that survive palaeosol formation, probably due to their tough, silica-imbued cell walls. Unfortunately, in the absence of attached leaves, they provide little information, other than demonstrating the abundance of equisetalean horsetail ferns in these latest Permian settings. *Paracalamites* stems are also one of the few plant body fossils that have been found in the lowermost Katberg Formation as defined here, eg. Bethel 763 in the Free State (Gastaldo et al, 2005; see later comments in Gastaldo et al., 2017).

*Glossopteris* leaf impressions occur in facies B at Spitskop (Figs 4 A–D) and are consistent with forms found at other latest Permian localities at Bethel 763 in the Free State,

the New and Old Wapadsberg Pass and Old Lootsberg Pass localities near Graaff Reinet in the Eastern Cape, and Ennersdale in KwaZulu-Natal in the eastern Karoo Basin (Gastaldo, 2005; Prevec et al. 2010; Gastaldo et al., 2017; pers. obs. R. Prevec). These leaves are typically elongate-lanceolate, strap-like and diminutive with fine-meshed, curved venation arching at a steep angle, similar to forms assigned by other authors to *Glossopteris angustifolia* Brongniart and *Glossopteris linearis* McCoy (e.g. Lacey et al., 1975; White, 1978).

The only fertile glossopterid specimens found at Spitskop, were several *Lidgettonia* cupules. Despite extensive bulk collecting at the Wapadsberg Pass localities (Prevec et al., 2010), the only glossopterid elements recovered were of this same leaf morphotype (referred to as W1) and *Lidgettonia* fructifications. The association between this leaf morphotype and fructifications of the Lidgettoniaceae has been previously documented in detail by Anderson and Anderson (1985) at numerous late Permian localities in KwaZulu-Natal, providing widespread and compelling evidence for their affiliation.

The discovery of a short shoot bearing the small, narrow leaves of *Glossopteris* morphotype W1, is of interest as it represents the first example of this morphotype preserved in attachment to a stem. The abscission scars on the shoot, the close, spiral arrangement of the leaves, the long leaf bases and the presence of rhombic bud-scales at the shoot terminus (Figs 4 C, D.), are consistent with *G. linearis*-bearing shoots reported by White (1978; fig. 4, p. 479) from the Upper Permian of Australia.

Several insect wings were found in association with the plant fossils in facies B on Spitskop, all of them grylloblattids (A. Nel, pers. comm., 2018). The best preserved of these is illustrated in Fig. 4G, and may belong to the Liomopteridae, one of the most abundant families in the upper Permian fossil record of KwaZulu-Natal (eg. Aristov and Mostovski, 2013).

On both Spitskop and Loskop, vertebrate fossils of the *Dapocephalus* AZ are fairly abundant in exposures of facies B. Specimens of *Lystrosaurus maccaigi* and *Dapocephalus leoniceps* (Fig. 5B) are relatively common, with *Dinanomodon rubidgei*, *Dicynodontoides recurvidens* and *L. curvatus* less so. Vertebrate fossils are typically preserved as isolated skulls, partially articulated cranial and postcranial remains, or isolated postcrania, with the notable exception of two near complete theriodont skeletons lying in close proximity to one another within massive siltstone on Spitskop. One specimen is a large (425 mm basal skull length) gorgonopsian (NMQR 4000) comprising a complete skull, vertebral column (to the pelvic girdle) and partial ribs, complete right and partial left scapula, both clavicles, coracoids, metacoracoids, sternum, partial ilia and right femur all in articulation, and a disarticulated humerus, ulna, radius and tibia. Approximately 15 cm away from this specimen lay an almost complete, articulated therocephalian, *Moschorhinus kitchingi* (NMQR 3939), with only the left manus, right forelimb, left hind limb, right pes, tail and left side of the pelvic girdle missing (Fig. 5C, D). The disarticulated postcranial bones from the gorgonopsian are scattered on either side of the *Moschorhinus* skeleton (Fig. 5C, D). The disarticulated gorgonopsian bones have all been moved in the same direction (i.e. towards the *Moschorhinus* skeleton), suggesting transportation by fluid flow rather than scavenger action. No tooth punctures or grooves were found on either skeleton. Interestingly, an isolated gorgonopsian femur was found near the base of the *Moschorhinus* skeleton, however the rest of the disarticulated gorgonopsian postcrania occurred approximately 10 cm higher up but still within the same bed, level with the top of the *Moschorhinus* skeleton. A comparable 3-D association of semi-articulated skeletons of two *Moschorhinus* and a *Lystrosaurus maccaigi* was described from the same stratigraphic level and in similar facies on Bethel 763 (Smith and Botha-Brink, 2014: p. 109), which was interpreted as a possible carnivore-rich miring

scenario similar to that of the Pleistocene Rancho La Brea bonebeds in California (Spencer et al., 2003).

A relatively large non-mammalian cynodont was also recovered from facies B. The material consists of cranial fragments (jugal, unidentifiable fragments), a lower jaw (partial dentary, articular), and some postcranial fragments. To date only one large non-mammalian cynodont has been described from the uppermost Permian, namely *Vetusodon elikhulu* (Abdala et al., 2019). Our specimen is more robust than *Procynosuchus* and may therefore represent *Vetusodon* (F. Abdala, pers. comm., 2019) or a particularly robust specimen of *Cynosaurus*.

#### *4.1.3. Facies C—Dark reddish-brown mudstone and olive-grey mudstone-siltstone couplets*

This easily recognisable facies (Fig. 3, Table 1, Supplementary Fig. S1, S3C–E, Supplementary Table S1) varies from just under 2 m thick on Loskop to approximately 3 m thick on Spitskop, but occurs at the same position in the facies sequence in both measured sections. The main sedimentological feature of this facies is the presence of distinctive thinly-bedded mudstone-siltstone couplets, each 1–3 cm thick, with a sharp flat basal surface and an upward fining texture. The coarser arenaceous siltstone beds are olive-grey (5Y4/2) whereas the mudstone laminae are dark reddish-brown (2.5YR 2.5/4). On Spitskop (Fig. 3, 19–22 m), the couplets change colour midway through the unit from dark reddish-brown mudstone and olive-grey siltstone to olive-grey mudstone and dark reddish-brown siltstone. Individual 2 cm-thick couplets can be traced laterally throughout the outcrop (approximately 8 m along strike on Spitskop) with no visible desiccation cracks, pedoturbation, calcite precipitation, or bioturbation (apart from isolated *Katbergia* burrows).

Fern occurrences in the late Permian fossil record are extremely rare, and have been limited until now to fragments of *Neomariopteris* (*Sphenopteris*) *lobifolia* from the

Wuchiapingian of KwaZulu-Natal (Lacey et al., 1975; Anderson and Anderson, 1985; Prevec et al., 2009). The few attached pinnules found in this facies at Spitskop are poorly preserved and the manner of pinnule attachment is unclear. In the absence of sporangia, a conclusive identification is not possible (Figs 4E, F). This is the first record of a fern from the Palingkloof Member of South Africa.

No vertebrate fossils were found in facies C at our study site. However, fragmented and isolated bones of the upper Permian taxa *Daptocephalus leoniceps*, *Lystrosaurus maccaigi*, *Dicynodontoides recurvidens* and *Moschorhinus kitchingi* have been found in this facies at the nearby Bethel 763, approximately 34 km to the southwest (Smith and Botha-Brink, 2014), where they represent the last occurrences of these animals, apart from *Moschorhinus*, in the sequence.

#### 4.1.4. Facies D—Massive silty-mudstone

This facies (Fig. 3, Table 1, Supplementary Fig. S1, Supplementary Table S1) comprises structureless dark reddish-brown silty-mudstone and olive-grey siltstone interbedded with minor thin fine-grained sandstone sheets. The tabular sheet sands are structured with horizontal to climbing ripple lamination and have distinctive sharp flat basal and upper contacts, the former commonly with sand-filled desiccation polygons and the latter preserving patches of claystone-veneered oscillation ripples (i.e., 13 m on Spitskop log of Fig 3). Horizons of rough-surfaced irregularly-shaped calcareous nodules and scattered small spherical glaebules (possible pisoliths) with internal shrinkage cracks are ubiquitous to these massive mudrock beds (Supplementary Fig S4A, B). The distinguishing sedimentological features of this facies include predominance of the dark reddish-brown (2.5 YR 2.5/4), massively bedded, silty mudstone, in contrast to the greyish-brown mudstone (2.5Y/2) of the lower facies. Upsection, this facies gives way to numerous thin beds of predominantly olive-

grey siltstone, which are ultimately truncated by the erosively-based conglomeratic sandstones of facies E of the Katberg Formation. The silt and sand-filled desiccation cracks and the presence of silt granules in the red mudrocks are interpreted as the first indication of aeolian dust in the depocentre. A loessic contribution to the thick massive silty-mudstone is supported by their uniform massive texture with planar or gently undulating contacts that are commonly veneered with claystone indicative of relatively rapid, episodic sedimentation (Giles et al., 2013). Weakly developed pedogenesis with textural BCa horizons showing claystone-lined shrink/swell planes and small spherical carbonate nodules are interpreted as immature loessic soils similar to the Triassic loessites described by Chan (1999) from the Ankareh Formation of north-central Utah.

Fossils within facies D at the study site include taxa typical of the Lower Triassic *Lystrosaurus* Assemblage Zone, namely *L. murrayi* (Fig. 6A), *L. declivis*, *L. curvatus* and the archosauriform *Proterosuchus fergusi* (Botha-Brink et al., 2014). The therocephalians *Olivierosuchus parringtoni* and *Moschorhinus kitchingi* have been found at this site by previous workers (Kitching, 1977; Botha-Brink et al., 2014), and our recent collecting has yielded articulated skeletons of *Tetracynodon darti* (Fig. 6B), as well as several indeterminate baurioids. Interestingly, cynodonts such as *Thrinaxodon* and *Galesaurus* that are relatively common in these facies on Bethel 763, have yet to be recovered from either Loskop or Spitskop.

A biostratigraphically important discovery is the recovery of five in-situ *L. maccaigi* specimens from Triassic facies D on both Loskop and Spitskop (Fig. 6C–E). Although *Lystrosaurus maccaigi* has been found in Triassic strata in Antarctica (Cosgriff et al., 1982), it was, until now, restricted to the latest Permian upper *Dapocephalus* AZ in the South African Karoo Basin where it was typically found at levels no higher than the lower Palingkloof Member (Botha and Smith, 2007; Smith and Botha-Brink, 2014; Viglietti et al.,

2016). Four of these new specimens were found in dark reddish-brown mudstone, at the same level as an *in situ* *L. murrayi* specimen on Loskop, approximately 7.5 m above the top of the mudstone/siltstone couplets of facies C (Fig. 3A, vertebrate numbers 20–23). The fifth specimen was found approximately 9 m above the facies C mudstone/siltstone couplets on Spitskop in an olive-grey siltstone (Fig. 3B, vertebrate number 40). The identification of these specimens as *L. maccaigi* is confirmed by the presence of relatively large, upward and forward facing orbits, prominent prefrontal and frontal bosses along the dorsal margin of the orbit, frontal rugosities, a sharply angled, relatively wide snout and generally higher cranial robustness compared to other *Lystrosaurus* species, regardless of body size (Brink, 1951; Cluver, 1971; Grine et al., 2006; Botha and Smith, 2007).

#### *4.1.5. Facies E—Conglomeratic sandstone / olive-grey mudrock*

This facies (Fig. 3, Supplementary Fig. S1, Supplementary Table S1) is composed of vertically-stacked, tabular, generally fine-medium-grained, light-grey sandstone bodies separated by intervals of upwardly thinning beds of blocky-weathering olive-grey siltstone and rare, fissile, dark reddish-brown mudstone. The thicker (3–5 m) multistoried channel sandstone bodies commonly display several (two to five) irregular accretion surfaces lined with platy mudrock clasts. A distinctive feature of this facies is elongate basal scours or gulleys eroded into the underlying mudrocks and filled with lenses of intraformational conglomerate (Supplementary Fig. S4C, D). The conglomerates are clast-supported and composed of mud pebbles, reworked bone fragments, irregular shaped pedogenic glaebules and smooth surfaced spheroidal pisoliths, many with distinctive internal septarian shrinkage cracks. Mudrock-dominated intervals comprise metre-thick beds of alternating fissile dark reddish brown and olive-grey mudstone with rare bodies of olive-grey siltstone interbedded with sporadic thin (0.25–0.5 m thick), light grey, fine-grained, single-storied, sheet sandstone

bodies, which commonly display sand-filled, downward tapering desiccation cracks at the basal contact. On both Spitskop and Loskop the dark reddish brown mudrocks change to predominantly olive-grey and olive colours higher up in facies D.

King (1961) and later Stavrakis (1980) first proposed that the vertically accreted multi-storied conglomeratic sandstone bodies in the Katberg Formation represented in-channel deposits of wide, shallow, low-sinuosity rivers with a highly fluctuating discharge regime. Hiller and Stavrakis (1984) later described the characteristics that indicated an arid fluvial setting, similar to what Smith and Botha-Brink (2014) have found. The presence of numerous, spherical, pea-sized, calcareous pisoliths (or glaebules) with septarian shrinkage cracks in the clast-supported melange of red mudrock pebbles, rolled bone fragments and other pedogenic calcareous nodules at Loskop and Spitskop, indicate that they too are reworked from the alluvium into which the channel has incised. The pisoliths are similar to those described from Quaternary calcretes of western Australia (Arakel, 1982) and the Indo-Gangetic alluvial plains of India (Khadkikar et al., 2000). In both instances they are formed by the repeated alternation between saturated and dry soil-moisture conditions under a warm climate, unpredictable rainfall regime. The appearance of similar septarian glaebules in the PTB stratigraphic record in the main Karoo Basin serves to strengthen the sedimentological facies interpretation for warm climatic conditions with highly seasonal rainfall in this part of western Gondwana in the earliest Triassic. Pace et al (2009) interpreted the pisolithic conglomerates as remnants of completely degraded landscapes. Whilst undoubtedly indicating floodplain abandonment and incision, we regard this as normal in arid zone fluvial systems and can find no evidence to support that these conglomerates record basinwide landscape degradation involving Milankovitch-scale time intervals.

Vertebrate fossils from facies E include taxa similar to those found in facies D, with increased predominance of *L. murrayi* and *L. declivis* specimens. *Lystrosaurus maccaigi* is

absent. The therocephalians *Tetracynodon darti* and *Scaloposaurus constrictus* (Fig. 6F) have also been recovered from the upper slopes of Spitskop, including articulated skeletons.

#### 4.2. Stable isotope results

Up to 40 metres of section from facies B–D records a period of relatively low  $\delta^{13}\text{C}_{\text{carbonate}}$  (V-PDB). The lowest  $\delta^{13}\text{C}_{\text{carbonate}}$  values were recovered from both carbonate nodules and theriodont enamel in facies B, immediately below the *Katbergia*-bearing couplets of facies C, where  $\delta^{13}\text{C}_{\text{carbonate}}$  values are generally not above -10.0 ‰ (Fig. 7; Supplementary Table S3). This precipitous negative excursion immediately preceding facies C, commonly yielding values below -10.0 ‰, has been recognised elsewhere in the Bethulie (MacLeod et al., 2000), Graaff Reinet (Gastaldo et al., 2014), and other study areas of the southern Karoo (Coney et al., 2007), and from composite sections of Karoo therapsid bioapatite (Rey et al., 2016). As with the carbon isotope data obtained from the nodules,  $\delta^{13}\text{C}_{\text{carbonate}}$  values from theriodont teeth obtained closer to facies C were generally more negative than those collected lower in section in the *Daptocephalus* AZ (Fig. 7).

Compared to the  $\delta^{13}\text{C}$  data,  $\delta^{18}\text{O}$  values showed fewer obvious trends in the Permian portion of the section. Nevertheless, values were slightly lower in the Permian samples (average,  $\delta^{18}\text{O}$ , -19.7 ‰<sub>V-PDB</sub>) than in the Triassic samples (average,  $\delta^{18}\text{O}$ , -16.2 ‰<sub>V-PDB</sub>). Elsewhere in the Bethulie area, primary  $\delta^{18}\text{O}$  values from carbonate nodules were also shown to become increasingly positive higher into the Triassic Katberg Formation, indicative of long-term Triassic climate warming (MacLeod et al., 2000, 2017). However, this portion of the section is not complete in our study area, constraining our sample to the underlying Balfour Formation (Palingkloof Member).

#### 4.3. Detrital zircon results

$^{206}\text{Pb}/^{238}\text{U}$  age profiles of detrital zircons (Fig. 8A–C, Supplementary Fig. S1, S2

Supplementary Table S4 University of Utah, S5 Stellenbosch University) yielded from facies B of the lower Palingkloof Member are consistent with a latest Permian major source and a maximum depositional age near the PTB. As many as four major modes were identified using LA-ICPMS (Fig. 8B), which included early and late Palaeozoic peaks, the largest peak attributed to a Permian-to-earliest-Triassic source (ca.  $298\text{--}249 \pm 2.7$  Ma,  $n = 38$ ; see Fig. 8B). We regard the latter peak as the youngest  $^{206}\text{Pb}/^{238}\text{U}$  ICPMS age due to minimum requirements of reproducibility (Dickinson and Gehrels, 2009). Of the 15 youngest zircons analyzed using ID-TIMS, the youngest five yielded a mean age of  $251.7 \pm 0.3$  Ma ( $2\sigma$ ; mean square of weighted deviates, MSWD = 0.63) (Fig. 8C; Supplementary Table S1). This overlaps the date of  $252.4 \pm 0.7$  Ma from boundary beds of the Palingkloof Member near Kommandodrift Dam (Eastern Cape Province) reported by Coney et al. (2007).

## 5. Discussion

### 5.1. Chronostratigraphy of the Palingkloof Member in the Xhariep District

The Permo-Triassic Beaufort Group succession contains what is arguably the best understood terrestrial PTB sequence in the world. Biostratigraphic studies focused on the tetrapod range zones of the Balfour and Katberg formations in the Eastern Cape and Free State (including the well-studied Xhariep District) established a three-phased extinction, with the main extinction pulse restricted to geologically “short lived” event beds in the Palingkloof Member of the Balfour Formation (Smith and Botha, 2005; Ward et al., 2005; Botha and Smith, 2006; Smith and Botha-Brink, 2014). Nevertheless, ongoing disputes over fossil taxon ranges and the lateral relationships of their host rocks, especially of the Palingkloof Member and Katberg Formation, have called into question the synchronicity of vertebrate extinctions

recorded across the Karoo, as well as their synchronicity with the global EPME (Gastaldo et al., 2009, 2014, 2015). Based on an analysis of sedimentation rates and ID-TIMS ages gleaned from porcellanite-derived zircons from the upper Elandsberg Member (underlying the Palingkloof Member) at Old Lootsberg Pass, Gastaldo et al. (2015) conjectured that the PTB may be situated higher in the Katberg Formation, and not in the Palingkloof Member where it is currently placed (Fig. 2). This would suggest that the entire extinction event occurred below the Permo-Triassic boundary.

It should be noted that the Old Lootsberg Pass site is biostratigraphically one of the most poorly constrained PTB sites, due to the paucity of vertebrate remains, and is taphonomically atypical with its relative abundance of plants (pers. obs., R. Prevec). Placement of the PTB is particularly challenging on the basis of both lithofacies analysis and vertebrate biostratigraphy. It is not immediately clear how Gastaldo et al. (2015) positioned the PTB on their lithostratigraphic log, as the reference they cited in support of this placement (Smith and Botha-Brink, 2014) only considered the Lootsberg Pass, further to the south-east, where a profusion of vertebrate fossils in addition to lithofacies analysis, facilitated confident placement of the boundary. Gastaldo et al. (2015) interpreted the stratigraphically lowermost occurrence of an intraformational pedogenic nodular conglomerate (PNC) at the Old Lootsberg Pass as a marker for the lower Triassic (either the upper Palingkloof or the base of the Katberg Formation), because this facies had been described by Botha and Smith (2006) from the upper Palingkloof at several PTB localities in the Free State. Although intraformational PNCs are certainly a characteristic of the upper Palingkloof Member at all of the PTB sites studied in South Africa, it has never been cited as a stand-alone indicator facies for the lower Triassic. It seems that Gastaldo et al. (2015) used this single first occurrence of PNC in the Old Lootsberg Pass to calibrate the entire PTB sequence at the site, extrapolating outwards using stratigraphic data transplanted from sections measured at the Lootsberg Pass

to the south-east. The single piece of biostratigraphic information available to them, viz. what they acknowledged to be a typically Permian dicynodont within the PNC itself, was used to propose the extension of the biostratigraphic range of the *Daptocephalus* AZ into the upper Palingkloof Member, instead of acknowledging the possibility that evidence of phases of regional water table fluctuation may be found earlier in the sequence than previously recognised.

Viglietti et al (2016, 2017, 2018a, 2018b) identified important palaeoenvironmental and biochronological changes indicative of the onset of the biotic crisis, already occurring below the phased extinctions of Smith and Botha-Brink (2014), and below the porcellanite of Gastaldo et al. (2015). This research supports the onset of a biotic crisis with the earlier extinction phases and the EPME occurring across this stratigraphic interval, and the authors caution against using sedimentation rates alone such as that used by Gastaldo et al. (2015) to infer chronostratigraphic boundaries (Fig. 2). This applies particularly when considering deposition during a time of great change in tectonics, climate and sedimentological regime in the Karoo Basin (Catuneanu et al., 2005; Viglietti et al., 2017).

The GSSP of the EPME near Meishan, South China, is well constrained at  $251.9 \pm 0.03$  Ma and is immediately preceded by a major  $\delta^{13}\text{C}_{\text{carbonate}}$  excursion on a scale of  $10^4$ – $10^5$  years (Shen et al., 2011, 2012, 2013; Burgess and Bowring, 2015; Baresel et al., 2017). Previous authors have argued that simultaneous isotopic shifts manifest in  $\delta^{13}\text{C}$  and  $\delta^{18}\text{O}$  records from Karoo pedogenic nodules and therapsid bioapatite, and that these shifts bear important climatic and geochronologic significance (e.g., MacLeod, 2000). Taken together with the  $\delta^{13}\text{C}$  data, corresponding long-term positive excursions in  $\delta^{18}\text{O}$  during the subsequent Triassic (Rey et al., 2016; MacLeod et al., 2017) have been linked to a more than 4–6 °C increase in global temperatures, as inferred from studies of several peri-Tethys marine sections (e.g., Joachimski et al., 2012; Sun et al., 2012; Schobben et al., 2014). Our high-

resolution geochemical evidence corroborates that the  $\delta^{13}\text{C}$  shift leading up to the PTB was indeed rapid in the Karoo Basin, and in our sampled portion of the Bethulie part of the basin, it showed a negative peak within the Palingkloof Member, some 10 to 20 m below the base of the Katberg Formation.

Our research at Nooitgedacht 68 and surrounding farms has consequently produced the first detailed vertebrate and floral collections within a terrestrial PTB sequence that are constrained by both relative (stable isotopes) and absolute (detrital zircon geochronology) dating methods. Latest Permian detrital zircons of Karoo-aged basins have been linked to Choyio volcanism in western Gondwana during this time (Sato et al., 2015; McKay et al., 2015). Notably, our age distributions from LA-ICPMS support such a source (Fig. 8B, Supplementary Fig. S1), and our mean age of  $251.7 \pm 0.3$  Ma based on ID-TIMS (Fig. 8C) overlaps with the only previous TIMS date reported from the Palingkloof Member more than 200 km south of the study area in the Eastern Cape (Coney et al., 2007). Both of these dates, however, are significantly younger than beds from the stratigraphically lower Elandsberg Member of Old Lootsberg Pass dated to  $253.4 \pm 0.15$  Ma (Gastaldo et al., 2015). Our zircon date corroborates that the uppermost strata of the Palingkloof Member in the Bethulie area are latest Permian but, within the margins of error of the calibration, it encompasses the Permo-Triassic boundary. Consequently, support for the placement of the PTB much higher in the succession within the Katberg Formation (Gastaldo et al., 2015), and much lower in the Old Lootsberg Pass, is lacking in the Bethulie area.

Further support for the synchronicity of the marine and terrestrial extinction events is provided by several studies from China (Chu et al., 2016, 2018, 2019) where these authors have found mixed continental-marine taxa from the post-extinction stratigraphic interval. These data provide biostratigraphical correlation between marine and continental PTB beds

and Chu et al. (2019) suggest that the assemblages may be considered as PTB transitional beds in marine-continental siliciclastic settings.

### 5.2 Identifying the terrestrial EPME interval in the Karoo Basin

We use a combination of features to identify the extinction interval in the South African Karoo Basin. The last appearance of the dicynodont therapsids *Dapocephalus leoniceps*, *Dicynodontoides recurvidens* and *Dinanomodon rubidgei* represents the disappearance of the uppermost Permian fauna. The first fossils of the *Lystrosaurus* AZ are typically found approximately 5 metres above the LAD of the *Dapocephalus* AZ fauna. These taxa include the archosauriform *Proterosuchus fergusi* and the dicynodonts *Lystrosaurus declivis* and *L. murrayi*. The latter two taxa are found by an order of magnitude in more abundance compared to any other vertebrates from the *Dapocephalus* and *Lystrosaurus* AZ, thus displaying typical features of disaster taxa in a post-extinction environment. *Lystrosaurus curvatus* and *L. maccaigi* as well as the therocephalians *Promoschorhynchus platyrhinus* and *Moschorhinus kitchingi* are found throughout this interval throughout the Karoo Basin. This faunal turnover is found in association with the transition from *Glossopteris*-dominated flora to *Dicroidium*-dominated flora. Specimens of *Glossopteris* may be found above the vertebrate extinction interval and *Dicroidium* below, but it is the change from predominantly *Glossopteris* to predominantly *Dicroidium* flora that is found at this interval. A series of very thin, alternating dark reddish-brown and olive-grey mudstone-siltstone couplets are found in association with the faunal turnover, which represent periodic drying and wetting of small ephemeral water bodies. The presence of these couplets at most PTB sites in the Karoo Basin does not suggest that a single large water body covered the Karoo region, but that numerous small ephemeral water bodies were becoming the norm over the large, high sinuosity, permanent rivers of the upper Permian. Mudstone-

siltstone couplets have been found at other stratigraphic levels in the upper Palingkloof Member, but they are not associated with the biotic extinction interval, making these particular couplets unique. These couplets are also found in association with a negative  $\delta^{13}\text{C}$  excursion at or just below the extinction interval. It is the combination of these features that allows for the identification of this interval as the terrestrial expression of the EPME and coincides with facies C. The same facies has been logged in the same sequence at all the southern PTB sections in the Sarah Baartman (previously Graaff-Reinet and Nieu Bethesda) District as well as at the northern section at Bethel 763 in the Xhariep District. Our ID-TIMS date supports this interpretation.

The extinction interval represents a transition zone and thus, it is difficult to draw a line within the zone. The top of the extinction interval originally coincided with the PTB and was originally placed at the bottom of facies C when it was first described (Smith and Ward, 2001), but after the recovery of *Lystrosaurus maccaigi* and *Moschorhinus kitchingi* within the mudstone-siltstone couplets it and the PTB were placed at the top of this facies because these taxa were thought to be entirely Permian. Further collecting has shown these taxa to be survivors of the EPME as specimens have also been recovered from the upper Palingkloof Member. Given that the last Permian taxa (*Dapocephalus leoniceps* and *Dicynodontoides recurvidens*) have been recovered from the middle of facies C we now place the PTB at the centre from the transition from predominantly dark reddish-brown to predominantly olive-grey mudstone-siltstone couplets. Further radiometric dating may further constrain the position of the boundary. The extinction interval is considered a transition zone and a line was only drawn in previous work and this study to make it easier to place the fossils on the lithostratigraphic logs.

### 5.3. Palaeoenvironment and palaeoecology

Global responses to the terrestrial EPME appear to have been varied, similar to those found in the marine realm. For example, despite a recent literature-based study suggesting that land plants did not experience a mass extinction because generic diversity remained fairly constant across the PTB (Nowak et al., 2019), another recent study, using empirical palynological and geochemical data collected from the Sydney Basin in Australia, proposed that the floral extinction began as soon as 252.3 Ma, some 400 000 years prior to the main marine extinction (Fielding et al., 2019). Fielding et al. (2019) also found no evidence of aridification in the Sydney Basin, in contrast to what has been reported for the Karoo Basin (Smith 1995; Smith and Ward 2001; Smith and Botha 2005; Smith and Botha-Brink, 2014). Although Retallack et al. (2003) and Tabor et al. (2007) suggested increased precipitation during the earliest Triassic, the conclusions in these studies have since been debated due to the unreliability of the methods used (in the case of Retallack et al., 2003, see Tabor et al., 2018) or independent evidence for increased aridity has been found using further geochemical analysis (MacLeod et al., 2017).

Li et al. (2017) collected data from Old Lootsberg Pass and argued against increased aridity as their investigation suggested that the increased reddening near the boundary (which is caused by the high incidence of Fe<sup>3+</sup> in an oxidizing environment indicating a dry climate and low water table) was due to diagenesis and not related to the climate. However, colour is only one feature that may be used as supporting evidence for the presence of aridity. Sedimentological evidence for increased aridity in the Early Triassic at all Karoo PTB sites studied to date includes the presence of claystone breccias, spheroidal glaebules with septaria, sand-filled desiccation cracks, rough-surfaced ferricrete and rhizocretions. Taphonomic evidence for aridity includes a high concentration of carcasses alongside floodplain deposits, numerous *Lystrosaurus* bonebeds containing disarticulated skeletons within floodplain depressions, mummified carcasses and vertebrate burrow casts. These features do not indicate

the absence of wet conditions, but that flooding events were interspersed with long periods of extreme drought.

Fielding et al. (2019) did find increased seasonality leading to the EPME with warmer summer temperatures in the Early Triassic similar to what has been found in South Africa and the differences in aridity are likely due to the Sydney Basin being closer to the coast compared to the Karoo Basin. In Australia, coal seams occur right up to the end of the Permian, which indicates that conditions in Australia were much wetter than in the Karoo basin, even before the onset of EPME-linked climate change (Michaelsen, 2002; Fielding et al, 2019). Heterogeneity of environmental conditions across the globe would have led to differing responses in both the floras and faunas from region to region.

Notably, we found *Glossopteris* impression fossils at Spitskop up to 9 m below facies C and Gastaldo et al. (2015, 2017) even reported *Glossopteris* from the Early Triassic *Lystrosaurus* AZ, although the vertebrate used to identify the assemblage zone at the position in which the *Glossopteris* was found is equivocal (see Viglietti et al., 2016), and their placement of the PTB was based on different criteria to those used by previous workers. It is clear, however, that *Glossopteris* fossils occur within the vertebrate-defined three-phased extinction zone.

The *Glossopteris* leaf morphotype tends to be smaller in size in the uppermost Permian compared to those lower down in the Wuchiapingian (Lacey et al., 1975; Anderson and Anderson 1985; Prevec et al., 2009, 2010). Prevec et al (2010) suggested that the diminutive size of the W1 *Glossopteris* morphotype could be a phenotypic response to potentially toxic ashfall associated with the Wapadsberg Pass deposits, or alternatively could reflect regional variation in this group of glossopterids. It seems most likely that this was a regional phenomenon, given the widespread occurrence of this small-leaved form that has been found as the dominant (and in most instances the only), leaf type in the uppermost

Permian Palingkloof Member at multiple sites across the Karoo Basin (Gastaldo et al, 2005, 2017; Prevec et al, 2010), and as far afield as Australia (Fielding et al, 2019; their fig. 2) and in India, where a general reduction in size of glossopterid leaves at the Permo-Triassic transition was also observed (Saxena et al, 2018). The tendency of plants to produce small, narrow leaves under water stress is a well-recognised phenotypic response, as is the tendency for plant communities to exhibit a low diversity. The prevalence of the W1 morphotype during the latest Permian of South Africa may have been the result of the general warming and drying of the climate or to the intensification of seasonal extremes in the prelude to and during the EPME.

The discovery of a fern impression from within the PTB transition zone at Spitskop represents the first pteridophyte found in the late Permian of the southern Karoo Basin. Additionally, the discovery of fern fragments in palaeosols is taphonomically highly unlikely. Given the very low odds of plant fossilization in these strata, it indicates that they were likely abundant, at least within this localized habitat during times of water availability.

Updating the biostratigraphic ranges of the recently recovered vertebrates moves the lower limit of Smith and Botha-Brink's (2014) Extinction Phase 2 slightly higher to 15 m below the boundary interval (Fig. 9). Our radiometric date of  $251.7 \pm 0.3$  Ma gives a maximum age of 252 Ma at 6.5 m below the extinction interval, suggesting that Phase 2 may have lasted as long as 300 000 years (similar to the onset of the floral extinction in the Sydney Basin, Fielding et al., 2019). We accept that our new date was derived from detrital rather than primary airfall tuff bed material and consequently has a large error margin. Until more datable tuff horizons are recovered from the Extinction Phase 2 interval, the duration of this phase must remain speculative. It is clear, however, that the vertebrate fossils collected from Loskop and Spitskop are indicative of the upper Permian *Daptocephalus* and Triassic *Lystrosaurus* AZ, and show facies associations (facies A–E) similar to those documented at

PTB sites in other areas of the Karoo Basin, suggesting that the facies and associated vertebrate succession reported in previous studies (e.g. Smith and Botha-Brink, 2014) were not isolated, local events (Fig. 10). Sites in the southern part of the Karoo Basin contain thicker facies compared to those in the northern part of the basin (Fig. 10), but the sequence of each facies and pattern of faunal extinctions remains similar. To account for the heterogenous nature of Karoo Basin strata, it is important to examine as many sites containing the extinction interval as possible. All sites studied to date have a suite of features that allow us to identify the extinction zone and conclude that the transition from Permian to Triassic ecosystems at these sites was essentially contemporaneous. However, each site also has unique characteristics that makes some sites clearer than others. The site at Old Lootsberg Pass, for example, is one such problematic site (based on the presence of a fault), which makes any data from this site dubious. There are, however, several other sites that do not have this problem, where the couplets (e.g. Bethel 763, Commandodrift Dam, Nooitgedacht 68), vertebrate biostratigraphy (e.g. Bethel 763, Old Wapadsberg, Nooitgedacht 68), geochemistry (e.g. Bethel 763, Carlton Heights, Nooitgedacht 68) etc. are particularly clear. We recommend utilizing all available information to define the extinction or transition zone, and caution against basing the position of the terrestrial PTB in the Karoo Basin on palaeomagnetic data alone (Gastaldo et al., 2015), given the abundance of dolerite dykes and sills affecting the data.

## 6. Conclusions

Multiple lines of evidence, including a new radiometric date, provide a compelling argument for the placement of the extinction interval within the Palingkloof Member of the Balfour Formation, Beaufort Group, Karoo Supergroup. These include the recognition of a distinctive sequence of facies from A–E that portray a consistent trend in sedimentary

features resulting from regional changes in climate and fluvial regimes, a strong ??<sup>13</sup>C negative excursion within facies C, and most critically, the same patterns in faunal and floral turnover within this interval. We suggest that facies C consistently coincides with the major end-Permian pulse of extinctions, and together with the rich associated fossil record of the Karoo Basin, presents the most consistent and compelling means of identifying the Permo-Triassic transition in South Africa.

## Acknowledgments

AKH thanks S. Blumenthal, K. Chritz, and the Cerling Stable Isotopes Laboratory at the University of Utah, Salt Lake City, for technical assistance during the stable isotope analysis. We also thank R. Irmis, D. Fernandez, and M. Stearns of the University of Utah, and R. Mundil of the Berkeley Geochronology Center for assistance with U-Pb detrital zircon dating. JB thanks M. Grobbelaar and L. Bracciali from the Central Analytical Laboratories, University of Stellenbosch for their aid in processing, analyzing and writing the detailed methodology for the LA-ICP-MS results. JB was funded by the National Research Foundation (GUN 98819), the DST-NRF Centre of Excellence in Palaeosciences (CoE-Pal) and the Palaeontological Scientific Trust (PAST). AKH has been funded by the National Science Foundation (*NSF-PRFB-1309040*). SPM was funded by an RP grant from Cape Breton University. RP was funded by the National Research Foundation (African Origins Platform, UID98822) and the DST-NRF Centre of Excellence in Palaeosciences (CoE-Pal).

## References

- Abdala, F., Gaetano, L.C., Smith, R.M.H., Rubidge, B.S., 2019. A new large cynodont from the Late Permian (Lopingian) of the South African Karoo Basin and its phylogenetic

- significance. *Zoological Journal of the Linnean Society*.  
<https://doi.org/10.1093/zoolinnean/zlz004>.
- Alonso-Zarza, A.M., 2003. Palaeoenvironmental significance of palustrine carbonates and calcretes in the geological record. *Earth-Science Reviews* 60, 261–298.
- Alroy, J., 2008. Dynamics of origination and extinction in the marine fossil record. *Proceedings of the National Academy of Sciences* 105, 11536–11542.
- Anderson, J.M., Anderson, H.M., 1985. Palaeoflora of southern Africa. *Prodromus of South African megafloras. Devonian to Lower Cretaceous*. Rotterdam, Balkema.
- Anderson, J.M., Anderson, H.M., Cleal, C.J. 2007. Brief history of the gymnosperms: classification, biodiversity, phytogeography and ecology. *Strelitzia* 20, South African National Biodiversity Institute, Pretoria.
- Arakel, A.V., 1982. Genesis of calcrete in Quaternary soil profiles, Hutt and Leeman lagoons, Western Australia. *Journal of Sedimentary Research* 52, 109–125.
- Arche, A., López-Gómez, J., 2005. Sudden changes in fluvial style across the Permian-Triassic boundary in the eastern Iberian Ranges, Spain: Analysis of possible causes. *Palaeogeography, Palaeoclimatology, Palaeoecology* 229, 104–126.
- Aristov, D.S., Mostovski, M.B., 2013. Grylloblattids (Insecta, Grylloblattida) from the Upper Permian of South Africa. *Paleontological Journal* 47, 495–502.
- Baresel, B., Bucher, H., Brosse, M., Cordey, F., Guodun, K., Schaltegger, U., 2017. Precise age for the Permian–Triassic boundary in South China from high-precision U-Pb geochronology and Bayesian age–depth modeling. *Solid Earth* 8(2), 361–378.
- Benton, M.J., Tverdokhlebov, V.P., Surkov, M.V., 2004. Ecosystem remodeling among vertebrates at the Permian-Triassic boundary in Russia. *Nature* 432, 97–100.

- Black, B.A., Elkins-Tanton, L.T., Rowe, M.C., Ukstins Peate, I., 2012. Magnitude and consequences of volatile release from the Siberian Traps. *Earth and Planetary Science Letters* 317–318, 363–373.
- Botha, J., Smith, R.M.H., 2006. Rapid vertebrate recuperation in the Karoo Basin following the End-Permian extinction. *Journal of African Earth Sciences* 45, 502–514.
- Botha J., Smith, R.M.H., 2007. *Lystrosaurus* species composition across the Permian-Triassic boundary of South Africa. *Lethaia* 40, 125–137.
- Botha-Brink, J., Huttenlocker, A.K., Modesto, S.P., 2014. Vertebrate Paleontology of Nootgedacht 68: A *Lystrosaurus maccagii*-rich Permian-Triassic boundary locality in South Africa. In: Kammerer, C.F, Angielczyk, K.D., Fröbisch, J. (Eds.), *The Early Evolutionary History of the Synapsida*. Springer, Dordrecht, Netherlands, pp. 289–304.
- Botha-Brink, J., Huttenlocker, A., Angielczyk, K.D., Codron, D., Ruta, M., 2016. Breeding young as a survival strategy during Earth's greatest mass extinction. *Scientific Reports* 6, 24053. <https://doi.org/10.1038/srep24053>.
- Brennecke, G.A., Herrmann, A.D., Algeo, T.J., Anbar, A.D., 2011. Rapid expansion of oceanic anoxia immediately before the end-Permian mass extinction. *Proceedings of the National Academy of Sciences USA* 108(43), 17631–17634.
- Brink, A.S., 1951. On the genus *Lystrosaurus* Cope. *Transactions of the Royal Society of South Africa* 33, 107–120.
- Burgess, S. D., Bowring, S.A., 2015. High-precision geochronology confirms voluminous magmatism before, during, and after Earth's most severe extinction. *Science Advances* 1(7), e1500470.
- Burgess, S.D., Bowring, S.A. Shen, S.-Z., 2014. High-precision timeline for Earth's most severe extinction. *Proceedings of the National Academy of Science* 111, 3316–3321.

- Burgess, S.D., Muirhead J.D., Bowring S.A., 2017. Initial pulse of Siberian Traps sills as the trigger of the end-Permian mass extinction. *Nature Communications*.  
<https://doi.org/10.1038/s41467-017-00083-9>.
- Cao, C., Wang, W., Liu, L., Shen, S., Summons, R.E., 2008. Two episodes of  $^{13}\text{C}$ -depletion in organic carbon in the latest Permian: Evidence from the terrestrial sequences in northern Xinjiang, China. *Earth and Planetary Science Letters*. 270, 251–257.
- Cascales-Minana B, Cleal CJ. 2014. The plant fossil record reflects just two great extinction events. *Terra Nova*. 26(3):195–200.
- Cascales-Miñana, B., Diez, J.B, Gerrienne, P., Cleal, C.J. 2016. A palaeobotanical perspective on the great end-Permian biotic crisis. *Historical Biology* 28:8, 1066–1074.
- Catuneanu O., Wopfner, H., Eriksson, P.G., Cairncross, B., Rubidge, B.S., Smith, R.M.H., Hancox, P.G. 2005. The Karoo basins of south-central Africa *Journal of African Earth Sciences* 43, 211–253.
- Chan, M.A., 1999. Triassic loessite of North-Central Utah: stratigraphy, petrophysical character, and paleoclimate implications. *Journal of Sedimentary Research* 69, 477–485.
- Chen, Z-q., Kaiho, K., George, A.D., 2005. Early Triassic recovery of the brachiopod faunas from the end-Permian mass extinction: A global review. *Palaeogeography, Palaeoclimatology, Palaeoecology* 22, 270–290.
- Chu, D.L., Yu, J.X., Tong, J.N., Benton, M.J., Song, H.J., Huang, Y.F., Song, T., Tian, L., 2016. Biostratigraphic correlation and mass extinction during the Permian-Triassic transition in continental-marine siliciclastic settings of South China. *Global and Planetary Change* 146, 67–88.

- Chu, D.L., Yu, J.X., Tong, J.N., Benton, M.J., Song, H.J., Huang, Y.F., Song, T., and Tian, L. 2018. Biostratigraphic correlation and mass extinction during the Permian-Triassic transition in terrestrial-marine siliciclastic settings of South China. *Global and Planetary Change* 146, 67-88. <https://doi: 10.1016/j.gloplacha.2016.09.009>.
- Chu, D.L., Tong, J.N., Benton, M.J., Yu, J.X., and Huang, Y.F. 2019. Mixed continental-marine biotas following the Permian-Triassic mass extinction in South and North China. *Palaeogeography, Palaeoclimatology, Palaeoecology* 519, 95-107. <https://doi: 10.1016/j.palaeo.2017.10.028>.
- Clarkson, M.O., Richoz, S., Wood, R.A., Maurer, F., Krystyn, L., McGurty, D.J., Astratti, D., 2013. A new high-resolution  $\delta^{13}\text{C}$  record for the Early Triassic: Insights from the Arabian Platform. *Gondwana Research* 24, 233–242.
- Cluver, M.A., 1971. The cranial morphology of the dicynodont genus *Lystrosaurus*. *Annals of the South African Museum* 56, 155–274.
- Collinson, J.W., Hammer, W.R., Askin, R.A., Elliot, D.H., 2006. Permian-Triassic boundary, central Transantarctic Mountains, Antarctica, *Geological Society of America Bulletin* 118, 747–763.
- Coney, L., Reimold, W.U., Hancox, P.J., Mader, D., Koeberl, C., McDonald, I., Struck, U., Vajda, V., Kamo, S.L., 2007. Geochemical and mineralogical investigation of the Permian-Triassic boundary in the continental realm of the southern Karoo Basin, South Africa. *Palaeoworld* 16, 67–104.
- Cosgriff, J.W., Hammer, W.R. Ryan, W.R., 1982. The Pangaean reptile, *Lystrosaurus maccaigi*, in the Lower Triassic of Antarctica. *Journal of Paleontology* 56, 371–385.
- Cui, Y., Bercovici, A., Yu, J., Kump, L.R., Freeman, K.H., Su, S., Vajda, V., 2017. Carbon cycle perturbation expressed in terrestrial Permian-Triassic boundary sections in South China. *Global and Planetary Change* 148, 272–285.

- Dickinson, W.R., Gehrels, G.E., 2009. Use of U-Pb ages of detrital zircons to infer maximum depositional ages of strata: a test against a Colorado Plateau Mesozoic database. *Earth and Planetary Science Letters* 288, 115–125.
- Erwin, D.H., Bowring, S.A., Yugan, J., 2002. End-Permian mass extinctions: A review. In: Koeberl, C., MacLeod, K.G., (Eds.), *Catastrophic Events and Mass Extinctions: Impacts and Beyond*, Boulder, Colorado, Geological Society of America Special Paper 356, pp. 363–383.
- Fielding, C.R., Frank, T.D., McLoughlin, S., Vajda, V., Mays, C., Tevyaw, A.P., Winguth, A., Winguth, C., Nicoll, R.S., Bocking, M., Crowley, J.L., 2019. Age and pattern of southern high-latitude continental end-Permian extinction constrained by multiproxy analysis. *Nature Communications* 10:385. <https://doi.org/10.1038/s41467-018-07934-z>.
- Foster, W.J., Twitchett, R.J., 2014. Functional diversity of marine ecosystems after the Late Permian mass extinction event. *Nature Geoscience* 7, 233–238.
- Fröbisch, J., 2013. Vertebrate diversity across the end-Permian mass extinction—separating biological and geological signals. *Palaeogeography, Palaeoclimatology, Palaeoecology* 372, 50–61.
- Gastaldo, R.A., Rolerson, M.W., 2008. *Katbergia* gen. nov., a new trace fossil from Upper Permian and Lower Triassic rocks of the Karoo Basin: implications for palaeoenvironmental conditions at the P/Tr Extinction event. *Palaeontology* 51(1), 215–229.
- Gastaldo, R.A., Adendorff, R., Bamford, M., Labandeira, C.C., Neveling, J., Sims, H., 2005. Taphonomic trends of macrofloral assemblages across the Permian-Triassic boundary, Karoo Basin, South Africa. *Palaios* 20, 479–497.

- Gastaldo, R.A., Neveling, J.C., Kittinger, C., Newbury, S.S., 2009. The terrestrial Permian–Triassic boundary event bed is a nonevent. *Geology* 37, 199–202.
- Gastaldo, R.A., Knight, C.L., Neveling, J., Tabor, N.J., 2014. Latest Permian paleosols from Wapadsberg Pass, South Africa: Implications for Changhsingian climate. *GSA Bulletin* 126, 665–679.
- Gastaldo, R.A., Kamo, S.L., Neveling, J., Geissman, J.W., Bamford, M., Looy, C.V., 2015. Is the vertebrate-defined Permian-Triassic boundary in the Karoo Basin, South Africa, the terrestrial expression of the end-Permian marine event? *Geology* 43, 939–942.
- Gastaldo, R.A., Neveling, J., Looy, C.V., Bamford, M., Kamo, S.L., Geissman, J.W., 2017. Paleontology of the Blaauwater 67 and 65 farms, South Africa: testing the *Dapocephalus/Lystrosaurus* biozone boundary in a stratigraphic framework. *Palaios* 32, 349–366.
- Gastaldo, R.A., Neveling, J., Geissman, J.W., Li, J., 2019. A multidisciplinary approach to review the vertical and lateral facies relationships of the purported vertebrate-defined terrestrial Permian–Triassic boundary interval at Bethulie, Karoo Basin, South Africa. *Earth-Science Reviews* 189, 220–243.  
<https://doi.org/10.1016/j.earscirev.2017.08.002>.
- Giles, J.A., Soreghan, M.J., Benison, K.C., Soreghan, G.S., Hasiotis, S.T., 2013. Lakes, loess and paleosols in the Permain Wellington Formation of Oklahoma, USA: implications for palaeoclimate and palaeogeography of the midcontinent. *Journal of Sedimentary Research* 83, 825–846.
- Gradstein, F.M., Ogg, J.G., Hilgen, F.J., 2012. On the geologic time scale. *Newsletter on Stratigraphy* 45, 171–188.
- Grasby, S.E., Sanei, H., Beauchamp, B., 2011. Catastrophic dispersion of coal fly ash into oceans during the latest Permian extinction. *Nature Geoscience* 4, 104–107.

- Grauvogel-Stamm, L., Ash, S.R., 2005. Recovery of the Triassic land flora from the end-Permian life crisis. *Comptes Rendus Palevol* 4, 593–608.
- Grine, F.E., Forster, C.A., Cluver, M.A., Georgi, J.A., 2006. Cranial variability, ontogeny and taxonomy of *Lystrosaurus* from the Karoo Basin of South Africa. In: Carrano, M., Blob, R.W., Gaudin, T.J., Wible, J.R., (Eds.). *Amniote Paleobiology: Perspectives on the Evolution of Mammals, Birds, and Reptiles*. University of Chicago Press, Chicago, pp. 403–503.
- Hancox, P.J., Brandt, D., Reimold, W.U., Koeberl, C., Neveling, J., 2002. Permian-Triassic boundary in the northwest Karoo basin: Current stratigraphic placement, implications for basin development models, and the search for evidence of impact. In: Koeberl, C., MacLeod, K.G., (Eds.), *Catastrophic Events and Mass Extinctions: Impacts and Beyond*, Boulder, Colorado, Geological Society of America Special Paper 356, pp. 429–444.
- Hiller, N., Stavrakis, N., 1984. Permo-Triassic fluvial systems in the southeastern Karoo basin, South Africa. *Palaeogeography, Palaeoclimatology, Palaeoecology* 45, 1–21.
- Huttenlocker, A. K., 2013. The paleobiology of South African therapsids (Amniota, Synapsida) and the effects of the end-Permian extinction on size, growth, and bone microstructure. PhD Dissertation, University of Washington, 414 pp.
- Huttenlocker, A.K., 2014. Body size reductions in nonmammalian eutheriodont therapsids (Synapsida) during the End-Permian mass extinction. *PLoS ONE* 9(2), e87553.
- Huttenlocker, A. K., Botha-Brink, J., 2013. Body size and growth patterns in the therapsid *Moschorhinus kitchingi* (Therapsida: Eutheriodontia) before and after the end-Permian extinction in South Africa. *Paleobiology* 39(2), 253–277.

- Huttenlocker, A. K., Botha-Brink, J., 2014. Bone microstructure and the evolution of growth patterns in Permo-Triassic therocephalians (Amniota, Therapsida) of South Africa. PeerJ 2, e325.
- Huttenlocker, A. K., Sidor, C.A., Smith, R.M., 2011. A new specimen of *Promoschorhynchus* (Therapsida: Therocephalia: Akidnognathidae) from the Lower Triassic of South Africa and its implications for theriodont survivorship across the Permian-Triassic boundary. Journal of Vertebrate Paleontology, 31(2), 405–421.
- Irmis, R.B., Whiteside, J.H., 2011. Delayed recovery of non-marine tetrapods after the end-Permian mass extinction tracks global carbon cycle. Proceedings of the Royal Society B, 279. <http://doi.org/10.1098/rspb.2011.1895>.
- Irmis, R.B., Whiteside, J.H., Kammerer, C.F., 2013. Non-biotic controls of observed diversity in the paleontologic record: an example from the Permo-Triassic Karoo Basin of South Africa. Palaeogeography, Palaeoclimatology, Palaeoecology, 372, 62–77.
- Jackson II, R.G., 1981. Sedimentology of muddy fine-grained channel deposits in meandering streams of the American Middle West. Journal of Sedimentary Petrology 51, 1169–1192.
- Jin Y.G., Wang, Y., Wang, W., Shang, Q.H., Cao, C.Q., Erwin, D.H., 2000. Pattern of marine mass extinction near the Permian-Triassic boundary in South China. Science 289, 432–436.
- Joachimski, M.M., Lai, X.L., Shen, S.Z., Jiang, H.S., Luo, G.M., Chen, B., Chen, J., Sun, Y.D., 2012. Climate warming in the latest Permian and the Permian-Triassic mass extinction: Geology, 40, 195–198. <http://doi.org/10.1130/G32707.1>.
- Johnson, M.R., 1976. Stratigraphy and sedimentology of the Cape and Karoo Sequences in the Eastern Cape Province. Unpublished PhD thesis, Rhodes University, 336 pp.

- Kammerer, C.F., 2019. Revision of the Tanzanian dicynodont *Dicynodon huenei* (Therapsida: Anomodontia) from the Permian Usili Formation. PeerJ e7420.
- Kammerer, C.F., Angielczyk, K.D., Frobisch, J., 2011. A comprehensive taxonomic revision of *Dicynodon* (Therapsida, Anomodontia) and its implications for dicynodont phylogeny, biogeography, and biostratigraphy. Society of Vertebrate Paleontology Memoir 11 31, 1–158.
- Kerp, H., Hamad, A.A., Vörding, B., Bandel, K. 2006. Typical Triassic Gondwanan floral elements in the Upper Permian of the paleotropics. Geology 34(4), 265–268.
- Khadkikar, A.S., Merh, S.S., Malik, J.N., ChaMal, L.S., 1998. Calcretes in Semi-Arid Alluvial Systems: Formative Pathways and Sinks. Sedimentary Geology 116, 251–260.
- Khadkikar, A.S., ChaMal, L.S., Ramesh, R., 2000. The character and genesis of calcrete in Late Quaternary alluvial deposits, Gujarat, western India, and its bearing on the interpretation of ancient climates. Palaeogeography, Palaeoclimatology, Palaeoecology 162, 239–261.
- King, L.C., 1961. The Palaeoclimatology of Gondwanaland during the Palaeozoic and Mesozoic eras. In: Nairn, E.M (Ed), Descriptive Paleoclimatology. Interscience New York, pp. 307–331.
- Kitching, J.W., 1977. Distribution of the Karoo vertebrate fauna. Bernard Price Institute for Palaeontological Research Memoir 1, 1–131.
- Klappa, C.F., 1980. Rhizoliths in terrestrial carbonates: classification, recognition, genesis and significance. Sedimentology 27, 613–629.
- Korte, C., Kozur, H.W., 2010. Carbon-isotope stratigraphy across the Permian-Triassic boundary: A review. Journal of Asian Earth Sciences 39, 215–235.

- Labrecque, P.A., Hubbard, S.M., Jensen, J.L., Nielsen, H., 2011. Sedimentology and stratigraphic architecture of a point bar deposit, Lower Cretaceous McMurray Formation, Alberta, Canada. *Bulletin of Canadian Petroleum Geology* 59, 147–171.
- Lacey, W.S., van Dijk, D.E., Gordon-Gray, K.D., 1975. Fossil plants from the Upper Permian in the Mooi River district of Natal, South Africa. *Annals of the Natal Museum* 22, 349–420.
- Lau, K.V., Maher, K., Altiner, D., Kelley, B.M., Kump, L.R., Lehrmann, D.J., Silva-Tamayo, J.C., Weaver, K.L., Yu, M., Payne, J.L., 2016. Marine anoxia and delayed Earth system recovery after the end-Permian extinction. *Proceedings of the National Academy of Sciences*. <http://www.pnas.org/cgi/doi/10.1073/pnas.1515080113>.
- Li, J., Gastaldo, R.A., Neveling, J., Geissman, J.W., 2017. Siltstones Across the *Dapocephalus (Dicynodon)* and *Lystrosaurus* Assemblage Zones, Karoo Basin, South Africa, Show No Evidence For Aridification. *Journal of Sedimentary Research* 87, 653–671.
- Lindström, S., McLoughlin, S. 2007. Synchronous palynofloristic extinction and recovery after the end-Permian event in the Prince Charles Mountains, Antarctica: Implications for palynofloristic turnover across Gondwana. *Review of Palaeobotany and Palynology* 145, 89–122.
- Loope, G.R., Kump, L.R., Arthur, M.A., 2013. Shallow water redox conditions from the Permian–Triassic boundary microbialite: The rare earth element and iodine geochemistry of carbonates from Turkey and South China. *Chemical Geology* 351, 195–208.
- Looy, C.V., Twitchett, R.J., Dilcher, D.L., Van Konijnenburg-Van Cittert, J.H.A., Visscher, H., 2001. Life in the end-Permian dead zone. *Proceedings of the National Academy of Sciences* 98(14), 7879–7883.

- MacDougall, M.J., Brocklehurst, N., Fröbisch, J., 2019. Species richness and disparity of parareptiles across the end-Permian mass extinction. *Proceedings of the Royal Society B* 286: 20182572.
- MacLeod, G.K., Smith, R.M.H., Koch, P.L., Ward, P.D., 2000. Timing of mammal-like reptile extinctions across the Permian-Triassic boundary in South Africa. *Geology* 28, 227–230.
- MacLeod, G.K., Quinton, P.C., Bassett, D.J., 2017. Warming and increased aridity during the earliest Triassic in the Karoo Basin, South Africa. *Geology* 45(6), 483–486.
- McElwain JC, Punyasena SW. 2007. Mass extinction events and the plant fossil record. *Trends in Ecology and Evolution* 22(10), 548–557.
- McKay, M.P., Weislogel, A.L., Fildani, A., Brunt, R.L., Hodgson, D.M., Flint, S.S., 2015. U-Pb zircon tuff geochronology from the Karoo Basin, South Africa: implications of zircon recycling on stratigraphic age controls. *International Geology Review* 57(4), 393–410.
- Metcalfe, I., Foster, C.B., Afonin, S.A., Nicoll, R.S., Mundill, R., Xiaofeng, W., Lucas, S.G., 2009. Stratigraphy, biostratigraphy and C-isotopes of the Permian-Triassic non-marine sequence at Dalongkou and Lucaogou, Xinjiang Province, China. *Journal of Asian Earth Sciences*. 36, 503–520.
- Metcalfe, I., Crowley, J., Nicoll, R.S., Schmitz, M., 2015. High-precision U-Ph CA-TIMS calibration of middle Permian to Lower Triassic sequences, mass extinction and extreme climate-change in Eastern Australian Gondwana. *Gondwana Research* 28, 61–81.
- Michaelsen, P., 2002. Mass extinction of peat-forming plants and the effect on fluvial styles across the Permian-Triassic boundary, northern Bowen Basin, Australia. *Palaeogeography Palaeoclimatology Palaeoecology* 179, 173–188.

Nesbitt, S.J., Barrett, P.M., Werning, S., Sidor, C.A., Charig, A.J., 2013. The oldest dinosaur? A Middle Triassic dinosauriform from Tanzania. *Biology Letters* 9.

<http://doi.org/10.1098/rsbl.2012.0949>.

Newell, A.J., Tverdokhlebov, V.P., Benton, M.J., 1999. Interplay of tectonics and climate on a transverse fluvial system, Upper Permian, southern Uralian foreland basin, Russia. *Sedimentary Geology* 127, 11–29.

Nowak, H., Schneebeli-Hermann, E., Kustatscher, E., 2019. No mass extinction for land plants at the Permian-Triassic transition. *Nature Communications* 10:384.

<https://doi.org/10.1038/s41467-018-07945-w>.

Pace, D.W., Gastaldo, R.A., Neveling, J., 2009. Early Triassic aggradational and degradational landscapes of the Karoo Basin and evidence for climate oscillation following the P-Tr Event. *Journal of Sedimentary Research*, 79, 316–331.

<https://doi.org/10.2110/jsr.2009.036>.

Payne, J.L., Kump, L.R., 2007. Evidence for recurrent Early Triassic massive volcanism from quantitative interpretation of carbon isotope fluctuations. *Earth and Planetary Science Letters* 256, 264–277. *Science* 305, 506–508.

Payne, J.L., Lehrmann, D.J., Wei, J., Orchard, M.J., Schrag, D.P., Knoll, A.H., 2004. Large perturbations of the carbon cycle during recovery from the end-Permian extinction.

Prevec, R., Labandeira, C.C., Neveling, J., Gastaldo, R.A., Bamford, M.K., Looy, C.V., 2009. Portrait of a Gondwanan ecosystem: a new Late Permian locality from Kwazulu-Natal, South Africa. *Review of Palaeobotany and Palynology* 156, 454–493.

Prevec, R., Gastaldo, R.A., Neveling, J., Reid, S.B., Looy, C.V., 2010. An autochthonous glossopterid flora with latest Permian palynomorphs and its depositional setting in the *Dicroidium* Assemblage Zone of the southern Karoo Basin, South Africa. *Palaeogeography, Palaeoclimatology, Palaeoecology* 292(3-4), 391–408.

- Rees, P.M., 2002. Land-plant diversity and the end-Permian mass extinction. *Geology*, 30, 827–830.
- Renne, P.R., Zichao, Z., Richards, M.A., Black, M.T., Basu, A.R., 1995. Synchrony and causal relations between Permian–Triassic boundary crises and Siberian flood volcanism. *Science* 269, 1413–1416.
- Retallack, G.J. 1995. Permian–Triassic life crisis on land. *Science* 267, 77–80.
- Retallack GJ. 2013. Permian and Triassic greenhouse crises. *Gondwana Research* 24(1), 90–103.
- Retallack, G.J., Jahren, A.H., Sheldon, N.D., Chakrabarti, R., Metzger, C.A., Smith, R.M.H. 2005. The Permian-Triassic boundary in Antarctica. *Antarctic Science* 17, 241–258.
- Retallack, G.J., Seyedolali, A., Krull, E.S., Holser, W.T., Ambers C.P., Kyte, F.T., 1998. Search for evidence of impact at the Permian-Triassic boundary in Antarctica and Australia *Geology* 26(11), 979–982. <https://doi.org/10.1130/0091-7613>.
- Retallack, G.J., Smith, R.M.H., Ward, P.D., 2003. Vertebrate extinction across Permian–Triassic boundary in Karoo Basin, South Africa. *Geological Society of America Bulletin* 115, 1133–1152.
- Rey, K., Amiot, R., Fourel, F., Rigaudier, T., Abdala, F., Day, M.O., Fernandez, V., Fluteau, F., France-Lanord, C., Rubidge, B.S., Smith, R.M., Viglietti, P.A., Zipfel, B., Lécuyer, C., 2016. Global climate perturbations during the Permo-Triassic mass extinctions recorded by continental tetrapods from South Africa. *Gondwana Research* 37, 384–396.
- Rey, K., Amiot, R., Fourel, F., Abdala, F., Fluteau, F., Jalil, N.-E., Liu, J., Rubidge, B.S., Smith, R.M., Steyer, J.S., Viglietti, P.A., Wang, X., Lécuyer, C., 2017. Oxygen isotopes suggest elevated thermometabolism within multiple Permo-Triassic therapsid clades. *eLife* 6.

- Roopnarine, P.D., Angielczyk, K.D., 2012. The evolutionary palaeoecology of species and the tragedy of the commons. *Biology Letters* 8, 147–150.
- Roopnarine, P.D., Angielczyk, K.D., 2016. The stability of ecological communities as an agent of evolutionary selection. In: Eldredge, N., Pievani, T., Serrilli, E., Temkin, I., (Eds.), *Evolutionary Theory. A Hierarchical Perspective*, Chicago, University of Chicago Press, pp. 307–333.
- Roopnarine, P.D., Angielczyk, K.D., 2015. Community stability and selective extinction during the Permian-Triassic mass extinction. *Science* 350 (6256), 90–93.
- Roopnarine, P.D., Angielczyk, K.D., Wang, S.C., Hertog, R., 2007. Trophic network models explain instability of Early Triassic terrestrial communities. *Proceedings of the Royal Society B* 274, 2077–2086.
- Roopnarine, P.D., Angielczyk, K.D., Weik, A., Dineen, A., 2019. Ecological persistence, incumbency and reorganization in the Karoo Basin during the Permian-Triassic transition. *Earth-Science Reviews* 189, 244–263.
- Ruta, M., Benton, M.J., 2008. Calibrated diversity, tree topology and the mother of mass extinctions: the lesson of temnospondyls. *Palaeontology* 51, 1261–1288.
- Ruta, M., Botha-Brink, J., Mitchell, S.A., Benton, M.J., 2013a. The radiation of cynodonts and the ground plan of mammalian morphological diversity. *Proceedings of the Royal Society of London B* 280. <https://doi.org/10.1098/rspb.2013.1865>.
- Ruta, M., Angielczyk, K.D., Fröbisch, J., Benton, M.J., 2013b. Decoupling of morphological disparity and taxic diversity during the adaptive radiation of anomodont therapsids. *Proceedings of the Royal Society of London B* 280. <https://doi.org/10.1098/rspb.2013.1071>.
- Sanson-Barrera, A., Hochuli, P.A., Bucher, H., Schneebeli-Hermann, E., Weissert, H., Adatte, T., Bernasconi, S.M., 2015. Late Permian-earliest Triassic high-resolution

- organic carbon isotope and palynofacies records from Kap Stosch (East Greenland). Global and Planetary Change 133, 149–166.
- Sato, A.M., Llambías, E.J., Basei, M.A., Castro, C.E., 2015. Three stages in the Late Paleozoic to Triassic magmatism of southwestern Gondwana, and the relationships with the volcanogenic events in coeval basins. Journal of South American Earth Sciences 63, 48–69.
- Saxena, A., Singh, K. J., Cleal, C. J., Chandra, S., Goswami, S., Shabbar, H. 2018. Development of the *Glossopteris* flora and its end Permian demise in the Tatapani-Ramkola Coalfield, Son-Mahanadi Basin, India. Geological Journal.
- Schobben, M., Joachimski, M.M., Korn, D., Leda, L., Korte, C., 2014. Palaeotethys seawater temperature rise and an intensified hydrological cycle following the end-Permian mass extinction: Gondwana Research 26, 675–683.  
<https://doi.org/10.1016/j.gr.2013.07.019>.
- Shen, S-z, Crowley, J.L., Wang, Y., Bowring, S.A., Erwin, D.H., Sadler, P.M., Cao, C-q., Rothman, D.H., Henderson, C.M., Ramezani, J., Zhang, H., Shen, Y., Wang, X-d., Wang, W., Mu, L., Li, W-z., Tang, Y-g., Liu, X-l., Liu, L-j., Zeng, Y., Jiang, Y-f., Jin, Y-g., 2011. Calibrating the end-Permian mass extinction. Science 334, 1367–1372.
- Shen, J., Algeo, T. J., Hu, Q., Zhang, N., Zhou, L., Xia, W., Xie, S., Feng, Q., 2012. Negative C-isotope excursions at the Permian-Triassic boundary linked to volcanism. Geology 40(11), 963–966.
- Shen, S. Z., Cao, C. Q., Zhang, H., Bowring, S. A., Henderson, C. M., Payne, J. L., Davydov, V.I., Chen, B., Yuan, D-x., Zhang, Y-c., Wang, W., Zheng, Q-f., 2013. High-resolution  $\delta^{13}\text{C}_{\text{carb}}$  chemostratigraphy from latest Guadalupian through earliest Triassic in South China and Iran. Earth and Planetary Science Letters, 375, 156–165.

- Smith, R.M.H., 1987. Morphology and depositional history of exhumed Permian point-bars in the southwestern Karoo, South Africa. *Journal of Sedimentary Petrology* 57, 19–29.
- Smith, R.M.H., 1995. Changing fluvial environments across the Permian–Triassic boundary in the Karoo Basin, South Africa, and possible causes of the extinctions. *Palaeogeography, Palaeoclimatology, Palaeoecology* 117, 81–104.
- Smith, R.M.H., Botha, J., 2005. The recovery of terrestrial vertebrate diversity in South African Karoo basin after the End-Permian extinction. *Comptes Rendus Palevol* 4, 555–568.
- Smith R.M.H., Botha-Brink, J., 2014. Anatomy of a mass extinction: sedimentological and taphonomic evidence for drought-induced die-offs at the Permian-Triassic boundary in the main Karoo Basin, South Africa. *Palaeogeography, Palaeoclimatology, Palaeoecology*, 316, 99–118.
- Smith, R.M.H., Ward, P.D., 2001. Pattern of vertebrate extinctions across an event bed at the Permian–Triassic boundary in the Karoo Basin of South Africa. *Geological Society of America Bulletin* 29, 1147–1150.
- Spencer, L.M., Van Valkenburgh, B., Harris, J.M., 2003. Taphonomic analysis of large mammals recovered from the Pleistocene Rancho La Brea tar seeps. *Paleobiology* 29, 561–575.
- Stavrakis, N., 1980. Sedimentation of the Katberg Sandstone and Adjacent Formations in the South-Eastern Karoo Basin. *Transactions of the Geological Society of South Africa* 83, 361–374.
- Steiner M.B., Eshet Y., Rampino M.R., Schwindt, D.M., 2003. Fungal abundance spike and the Permian-Triassic boundary in the Karoo Supergroup (South Africa). *Palaeogeography, Palaeoclimatology, Palaeoecology*, 194, 405–414.

- Sun, Y.D., Joachimski, M.M., Wignall, P.B., Yan, C.B., Chen, Y.L., Jiang, H.S., Wang, L.N., Lai, X.L., 2012. Lethally hot temperatures during the Early Triassic greenhouse. *Science* 338, 366–370.
- Tabor, N.J., Montañez, I.P., Steiner, M.B., Schwindt, D., 2007.  $\delta^{13}\text{C}$  values of carbonate nodules across the Permian-Triassic boundary in the Karoo Supergroup (South Africa) reflect a stinking sulfurous swamp, not atmospheric CO<sub>2</sub>. *Palaeogeography, Palaeoclimatology, Palaeoecology* 252, 370–381.  
<https://doi.org/10.1016/j.palaeo.2006.11.047>.
- Tabor, N.J., Sidor, C.A., Smith, R.M.H., Nesbitt, S.J., Angielczyk, K.D., 2018. Paleosols of the Permian-Triassic: proxies for rainfall, climate change, and major changes in terrestrial tetrapod diversity. *Journal of Vertebrate Paleontology* 37(6), 240–253.
- Thomas, S.G., Tabor, N.J., Yang, W., Myers, T.S., Yang, Y., Wang, D., 2011. Palaeosol stratigraphy across the Permian-Triassic boundary, Bogda Mountains, NW China: Implications for palaeoenvironmental transition through earth's largest mass extinction. *Palaeogeography, Palaeoclimatology, Palaeoecology* 308, 41–64.
- Tripathi, C., Puri, S. N., 1961. On the remains of *Lystrosaurus* from the Panchets of the Raniganj coalfield. *Records of the Geological Survey of India* 89, 407–419.
- Tripathi, C., Puri, S. N., 1962. On the *Lystrosaurus* remains from Panchets of Raniganj Coalfield. *Records of the Geological Survey of India* 89(Pt 2), 407–23.
- Viglietti, P.A., Smith, R.M.H., Compton, J.S., 2013. Origin and palaeoenvironmental significance of *Lystrosaurus* bonebeds in the earliest Triassic Karoo Basin, South Africa. *Palaeogeography, Palaeoclimatology, Palaeoecology* 392, 9–21.
- Viglietti, P.A., Smith, R.M.H., Angielczyk, K.D., Kammerer, C.F., Fröbisch, J., Rubidge, B.S., 2016. The *Daptocephalus* Assemblage Zone (Lopingian), South Africa: A

proposed biostratigraphy based on a new compilation of stratigraphic ranges. Journal of African Earth Sciences 113, 1–12.

Viglietti, P.A., Rubidge, B.S., Smith, R.M.H., 2017. New Late Permian tectonic model for South Africa's Karoo Basin: foreland tectonics and climate change before the end-Permian crisis. Nature Scientific Reports 7, 10861. <https://doi.org/10.1038/s41598-017-09853-3>.

Viglietti, P.A., Smith, R.M., Rubidge, B.S., 2018a. Changing palaeoenvironments and tetrapod populations in the *Daptocephalus* Assemblage Zone (Karoo Basin, South Africa) indicate early onset of the Permo-Triassic mass extinction. Journal of African Earth Sciences 138, 102–111.

Viglietti, P.A., Frei, D., Rubidge, B.S., Smith, R.M., 2018b. U-Pb detrital zircon dates and provenance data from the Beaufort Group (Karoo Supergroup) reflect sedimentary recycling and air-fall tuff deposition in the Permo-Triassic Karoo foreland basin. Journal of African Earth Sciences, 143, 59–66.

Wang, Z., 1996. Recovery of vegetation from the terminal Permian mass extinction in North China. Review of Palaeobotany and Palynology 91, 121–142.

Ward, P.D., Montgomery, D.R., Smith, R.M.H., 2000. Altered river morphology in South Africa related to the Permian Triassic extinction. Science, 289(5485), 1740–1743.

Ward, P.D., Botha, J., Buick, R., De Kock, M.O., Erwin, D.H., Garrison, G.H., Kirschvink, J.L., Smith, R., 2005. Abrupt and gradual extinction among Late Permian land vertebrates in the Karoo Basin, South Africa. Science, 307(5710), 709–714.

Webb, J.A., Fielding, C.R., 1993. Permo-Triassic sedimentation within the Lambert Graben, northern Prince Charles Mountains, Antarctica. In: Finlay, R.H., Unrug, R., Banks, M.R., Veevers, J.J. (Eds.), Gondwana Eight. A.A. Balkema, Rotterdam, pp. 357–369.

- White, M. E., 1978. Reproductive structures of the Glossopteridales in the plant fossil collection of the Australian Museum. *Records of the Australian Museum* 31(12), 473–505.
- Wignall, P.B., Bond, D.P.G., Kuwahara, K., Kakuwa, Y., Newton, R.J., Poulton, S.W., 2010. An 80 million year oceanic redox history from Permian to Jurassic pelagic sediments of the Mino-Tamba terrane, SW Japan, and the origin of four mass extinctions. *Global Planet Change* 71(1-2), 109–123.
- Xie, S., Pancost, R.D., Yin, H., Wang, H., Evershed, R.P., 2005. Two episodes of microbial change coupled with Permo/Triassic faunal mass extinction. *Nature* 434, 494–497.
- Yang, W., Feng, Q., Liu, Y., Tabor, N., Miggins, D., Crowley, J.L., Lin, J., Thomas, S., 2010. Depositional environments and cyclo- and chronostratigraphy of uppermost Carboniferous–Lower Triassic fluvial-lacustrine deposits, southern Bogda Mountains, NW China – A terrestrial paleoclimatic record of mid-latitude NE Pangea. *Global and Planetary Change* 73, 15–113.
- Yin, H., Feng, Q., Lai, X., Baud, A., Tong, J., 2007. The protracted Permo-Triassic crisis and multi-episode extinction around the Permian-Triassic boundary. *Global and Planetary Change* 55, 1–20.
- Yu, J., Broutin, J., Chen, Z., Shi, X., Li, H., Chua, D., Huang, Q. 2015. Vegetation changeover across the Permian–Triassic Boundary in Southwest China Extinction, survival, recovery and palaeoclimate: A critical review. *Earth-Science Reviews* 149, 203–224.
- Zaton, M., Niedzwiedzki, G., Blom, H., Kear, B.P., 2016. Boreal earliest Triassic biotas elucidate globally depauperate hard substrate communities after the end-Permian mass extinction. *Scientific Reports* 6, 36345.

Zhang, H., Cao, C-q., Liu, X-l., Mu, L., Zheng, Q-f., Liu, F., Xiang, L., Liu, L-j., Shen, S-z.,  
2016. The terrestrial end-Permian mass extinction in South China. *Palaeogeography, Palaeoclimatology, Palaeoecology* 448, 108–124.

## Figure Captions

**Fig. 1.** Location of the study area. (A) Map of South Africa, star indicates the study area. (B) Map of the two study sites, Loskop and Spitskop. The red line surrounds the two sites, which cover three farms. (C) Outcrop of Loskop on the farm Nooitgedacht 68 (start of log  $30^{\circ}19'35.21''S\ 25^{\circ}55'53.71''E$ ). (D) Outcrop of Spitskop, which extends over the farms Nooitgedacht 68, Droogefontein 176 and Geluksfontein 204 (start of log  $30^{\circ}20'20.13''S\ 25^{\circ}55'32.25''E$ ). Right columns in (C) and (D) with A–E indicates the facies sequence through the PTB *sensu* Smith and Botha-Brink (2014), where A indicates massive greyish-brown mudrock, B massive mottled dark reddish brown/olive grey mudrock, C dark reddish-brown mudstone/olive-grey siltstone couplets, D massive silty-mudstone, E conglomeratic sandstone/olive mudrock facies. B: Bloemfontein; CT: Cape Town; D: Durban; EM: Elandsberg Member; F: Formation; JHB: Johannesburg; PM: Palingkloof Member; SM: Swartberg member. [2 column width]

**Fig. 2.** Stratigraphic position of the study area (in grey). AZ: Assemblage Zone; Bdp: Burgersdorp; Chs: Changhsingian; Fm: Formation; Mbr: Member. Dates follow Gradstein et al., 2012 and Burgess et al., 2014). [2 column width]

**Fig. 3.** Stratigraphic logs of (A) Loskop and (B) Spitskop up to the base of the Katberg Formation. A–E facies as in Fig. 1. See Table 1 for taxonomic identifications of the in situ fossils. Blue and red circles represent nodules taken for isotope analysis on Loskop and Spitskop, respectively. KF: Katberg Formation; PM: Palingkloof Member; PTB: Permian-Triassic boundary. [2 column width]

**Fig. 4.** Plant and insect fossils recovered from Spitskop. (A, B) Long, narrow *Glossopteris* leaves typical of the latest Permian Karoo Basin, showing abundant evidence of insect interactions in the form of prominent rows of elliptical oviposition scars (arrows) (N3-58a). (C) A short shoot with a whorl of *Glossopteris* leaves attached; the growth tip bears multiple attached rhombic bud scales (upper arrow), and leaf abscission scars are visible along the length of the shoot (lower arrow) (N3-35a). (D) Enlarged section of one of the attached leaves, showing typical glossopterid venation (N3-35c). (E, F) Indeterminate fern pinnules (N4-01). (G) One of several grylloblattid insect wing impressions (N3-9a). [2 column width]

**Fig. 5.** Permian tetrapod fossils from Loskop. (A) Dicynodont *Lystrosaurus maccaigi* NMQR 3647 (log number 13). (B) Dicynodont *Daptocephalus leoniceps* NMQR 3943. (C) Photograph and line drawing of gorgonopsian NMQR 4000 (green) (log number 9) and therocephalian *Moschorhinus kitchingi* NMQR 3939 (brown) (log number 8) found semi-articulated in close association with one another. (D) Enlargement of the articulated, almost complete skeleton of *Moschorhinus kitchingi* NMQR 3939. [2 column width]

**Fig. 6.** Early Triassic tetrapod fossils from Loskop and Spitskop. (A) Dicynodont *Lystrosaurus murrayi* NMQR 4152 (log number 24). (B) Therocephalian *Tetracynodon darti* NMQR 4160. (C) Dicynodont *L. maccaigi* NMQR 3689 (log number 22) lateral view. (D) Dicynodont *L. maccaigi* NMQR 3689 dorsal view. (E) Dicynodont *L. maccaigi* NMQR 3641 (log number 21). (F) Therocephalian *Scaloposaurus* NMQR 3923. C, clavicle; f, frontal; f b, frontal boss; f r, frontal rugosities; fe, femur; h, humerus; j, jugal; l, lacrimal; m, maxilla; n, nasal; p, parietal; pif, pineal foramen; pm, premaxilla; po, postorbital; prf, prefrontal; prf b,

prefrontal boss; r, radius, ri, rib; s, scapula; sq, squamosal; t, tibia; u, ulna; v, vertebra. [2 column width]

**Fig. 7.**  $\delta^{18}\text{O}$  and  $\delta^{13}\text{C}$  isotopes from pedogenic carbonate and theriodont therapsid tooth enamel plotted against the Loskop (blue) and Spitskop (red) stratigraphic logs. [1.5 column width]

**Fig. 8.** ICP-MS and TIMS analyses of detrital zircons from a volcaniclastic sandstone within the Palingkloof Member (Balfour Formation) at Spitskop. (A) Detrital zircons. (B) Four major modes were identified, the largest peak is attributed to Permian-to-earliest-Triassic sources. (C) Of the 15 youngest zircons, the youngest five yielded a mean age of  $251.7 \pm 0.3$  Ma. [1 column width]

**Fig. 9.** Summary figure of the end-Permian Mass Extinction in the South African Karoo Basin correlated with the marine extinction at Meishan, China. Radiometric dates: 1, Burgess et al., 2014; 2, this study. Terrestrial beds in metres, marine beds in centimetres. AZ, Assemblage Zone; Fm, Formation; Mbr, Member. [2 column width]

**Fig. 10.** Stratigraphic logs of the PTB logs from the southern to the northern part of the Karoo Basin (stars) on a map of South Africa showing similarities in the boundary interval from various parts of the basin. See Fig. 9 for facies A–E colours. Purple portion indicates Facies C, which contains the PTB in each log. Black arrows indicate the lower boundary of the Katberg Formation in all logs apart from the Verkykerskop log, which indicates the equivalent Verkykerskop Formation. Increments are in 10 metre intervals. B: Bloemfontein;

CT: Cape Town; D: Durban; GR: Graaff-Reinet. Sections adapted from Smith and Botha (2014) and Viglietti (2016). [2 column width]

**Declaration of interests**

The authors declare that they have no known competing financial interests or personal relationships that could have appeared to influence the work reported in this paper.

The authors declare the following financial interests/personal relationships which may be considered as potential competing interests:



**Table 1.** Identification, stratigraphic position and locality of the specimens numbered on the logs in Figure 3.

Log No.	Field No.	Accession Number	Taxon	PTB	Locality	Farm
VERTEBRATES						
1	JB031143	NMQR 3942	<i>Daptocephalus leoniceps</i>	-29	Loskop	Nooitgedacht 68
2	JB031137	NMQR 3938	<i>Lystrosaurus maccaigi</i>	-24	Loskop	Nooitgedacht 68
3	JB021030	NMQR 3706	<i>Lystrosaurus maccaigi</i>	-24	Loskop	Nooitgedacht 68
4	JB021013	NMQR 3694	<i>Lystrosaurus maccaigi</i>	-22	Loskop	Nooitgedacht 68
5	JB080813	NMQR 3644	<i>Daptocephalus leoniceps</i>	-21	Loskop	Nooitgedacht 68
6	JB080814	NMQR 3645	<i>Daptocephalus leoniceps</i>	-20	Loskop	Nooitgedacht 68
7	JB021032	OBSERVED	<i>Lystrosaurus maccaigi</i>	-16	Loskop	Nooitgedacht 68
8	JB031138	NMQR 3939	<i>Moschorhinus kitchingi</i>	-13.5	Loskop	Nooitgedacht 68
9	JB031138	NMQR 4000	Gorgonopidae	-13.5	Loskop	Nooitgedacht 68
10	JB031142	OBSERVED	<i>Lystrosaurus maccaigi</i>	-13.5	Loskop	Nooitgedacht 68
11	JB021024	NMQR 3701	<i>Daptocephalus leoniceps</i>	-12.5	Loskop	Nooitgedacht 68
12	JB031139	NMQR 3940	<i>Lystrosaurus maccaigi</i>	-12.5	Loskop	Nooitgedacht 68
13	JB080816	NMQR 3647	<i>Lystrosaurus maccaigi</i>	-12	Loskop	Nooitgedacht 68
14	JB031133	NMQR 3935	<i>Lystrosaurus maccaigi</i>	-11	Loskop	Nooitgedacht 68
15	JB021015	NMQR 3696	<i>Dinanomodon rubidgei</i>	-8	Loskop	Nooitgedacht 68
16	JB031134	NMQR 3936	<i>Lystrosaurus maccaigi</i>	-8	Loskop	Nooitgedacht 68
17	JB080815	NMQR 3646	<i>Lystrosaurus maccaigi</i>	-2	Loskop	Nooitgedacht 68
18	JB021012	NMQR 3693	<i>Lystrosaurus maccaigi</i>	5	Loskop	Nooitgedacht 68
19	JB021009	OBSERVED	<i>Lystrosaurus</i>	7	Loskop	Nooitgedacht 68
20	JB080818	NMQR 3648	<i>Lystrosaurus maccaigi</i>	7.5	Loskop	Nooitgedacht 68
21	JB080810	NMQR 3641	<i>Lystrosaurus maccaigi</i>	7.5	Loskop	Nooitgedacht 68
22	JB021006	NMQR 3689	<i>Lystrosaurus maccaigi</i>	7.5	Loskop	Nooitgedacht 68
23	JB021007	NMQR 3690	<i>Lystrosaurus maccaigi</i>	7.5	Loskop	Nooitgedacht 68
24	JB041642	NMQR 4152	<i>Lystrosaurus murrayi</i>	8	Loskop	Nooitgedacht 68
25	JB041625	NMQR 4175	<i>Lystrosaurus</i>	10	Loskop	Nooitgedacht 68
26	JB021008	NMQR 3691	<i>Lystrosaurus murrayi</i>	12	Loskop	Nooitgedacht 68
27	JB031123	NMQR 3928	<i>Lystrosaurus murrayi</i>	14	Loskop	Nooitgedacht 68
28	JB080835	NMQR 3663	<i>Lystrosaurus maccaigi</i>	-17	Spitskop	Nooitgedacht 68
29	JB080836	NMQR 3664	<i>Daptocephalus leoniceps</i>	-17	Spitskop	Droogefontein 176
30	JB031101	NMQR 3919	<i>Lystrosaurus maccaigi</i>	-17	Spitskop	Nooitgedacht 68
31	JB021045	NMQR 3713	<i>Lystrosaurus maccaigi</i>	-15.5	Spitskop	Droogefontein 176
32	JB031530	NMQR 4092	Cynodontia	-11	Spitskop	Nooitgedacht 68
33	JB031118	OBSERVED	<i>Lystrosaurus maccaigi</i>	-9	Spitskop	Droogefontein 176
34	JB031132	OBSERVED	<i>Daptocephalus</i>	-9	Spitskop	Droogefontein

			<i>leoniceps</i>			176
35	JB021036	NMQR 3707	Gorgonopidae	-8	Spitskop	Nooitgedacht 68
36	JB031107	NMQR 3922	<i>L. maccaigi &amp; L. curvatus</i>	-6	Spitskop	Droogefontein 176
37	JB031106	NMQR 3921	<i>Moschorhinus kitchingi</i>	-5	Spitskop	Droogefontein 176
38	RS 638	SAM-PK-K011534	tuskless dicynodont	-5	Spitskop	Droogefontein 176
39	JB031544	NMQR 4105	<i>Daptocephalus leoniceps</i>	-3	Spitskop	Geluksfontein 204
40	JB031534	NMQR 4095	<i>Lystrosaurus maccaigi</i>	9	Spitskop	Geluksfontein 204
41	JB041671	NMQR 4173	<i>Lystrosaurus curvatus</i>	11	Spitskop	Nooitgedacht 68
42	JB031117	OBSERVED	<i>Lystrosaurus</i>	11	Spitskop	Nooitgedacht 68
43	JB031105	OBSERVED	<i>Lystrosaurus</i>	12	Spitskop	Droogefontein 176
44	JB031104	NMQR 3920	<i>Lystrosaurus declivis</i>	12	Spitskop	Droogefontein 176
45	RS 641	SAM-PK-K011535	2 X <i>L. murrayi</i>	15	Spitskop	Geluksfontein 204
46	JB041658	NMQR 4164	<i>Lystrosaurus murrayi</i>	15	Spitskop	Nooitgedacht 68
47	JB041657	NMQR 4176	<i>Lystrosaurus murrayi</i>	15.5	Spitskop	Nooitgedacht 68
48	JB031109	OBSERVED	<i>Lystrosaurus</i>	16	Spitskop	Nooitgedacht 68
49	JB041664	OBSERVED	<i>Lystrosaurus</i>	16.5	Spitskop	Nooitgedacht 68
50	RS 640	OBSERVED	<i>Lystrosaurus declivis</i>	17	Spitskop	Nooitgedacht 68
51	JB031535	NMQR 4096	<i>Lystrosaurus declivis</i>	17	Spitskop	Nooitgedacht 68
PLANTS AND INSECTS						
Site W1			impression of tree branch (Botha-Brink et al., 2014)	-24	Loskop	Nooitgedacht 68
Site NP1			<i>Paracalamites</i>	-11.5	Spitskop	Droogefontein 176
Site NP2			<i>Glossopteris, Paracalamites</i>	-9	Spitskop	Droogefontein 176
Site NP3			<i>Glossopteris, Paracalamites, Trizygia, insect wings</i>	-11	Spitskop	Droogefontein 176
Site NP4			Fern rachis	0	Spitskop	Droogefontein 176

**Table 2.** Summary of  $^{206}\text{Pb}/^{238}\text{U}$  ages from Spitskop detrital zircons.

Sample Unit name	Relative age (global stage)	Major mode <sup>*</sup> (Ma)	Maximum age <sup>**</sup> (Ma)	$\pm 2\sigma$ <sup>**</sup> (Ma)	MSWD
Ka01 lower Palingkloof Member (Balfour Formation), facies B	Changxingian stage	298–249 ± 2.7 (n = 38)	251.7 (n = 5)	0.3	0.63

\*age profiles of multiple detrital zircon populations determined by LA-ICPMS results (the major mode reported here is also the youngest; see Fig. 8B);

\*\*based on youngest zircons selected from ID-TIMS

## Highlights

- A new site containing a complete sequence through the terrestrial PTB.
- A new radiometric date for the terrestrial end-Permian extinction.
- Data suggests the marine and terrestrial extinctions were synchronous.
- The current placement of the PTB in the Karoo Basin of South Africa is retained.

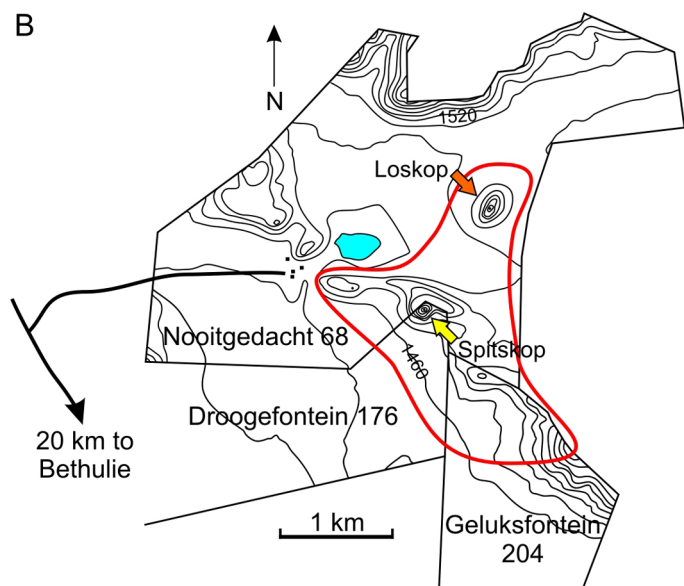
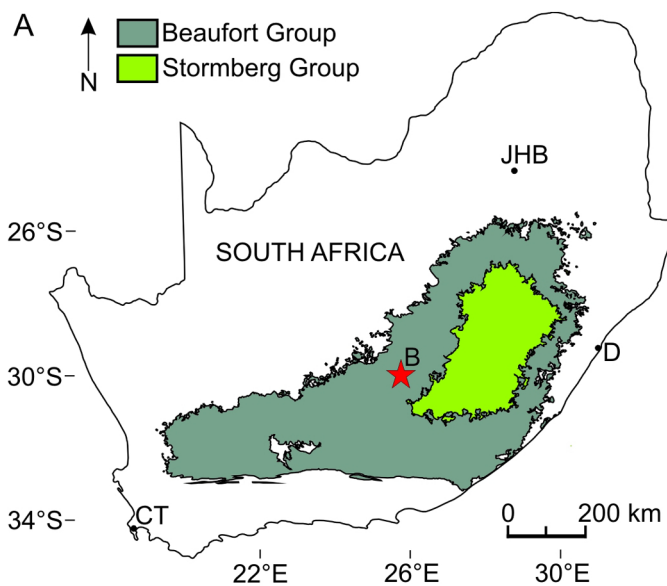


Figure 1

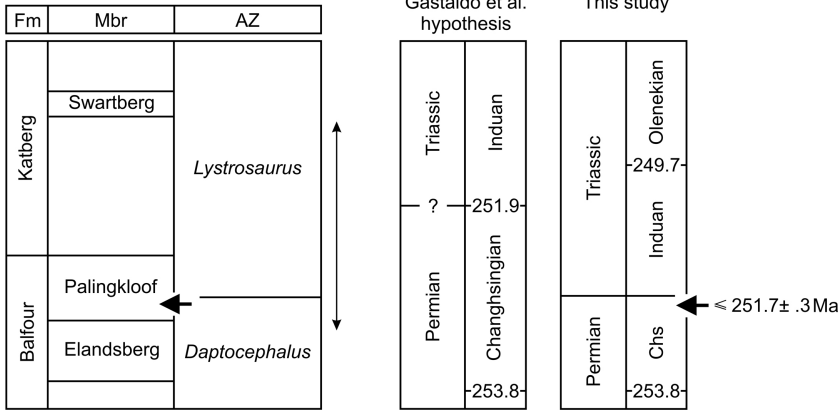


Figure 2

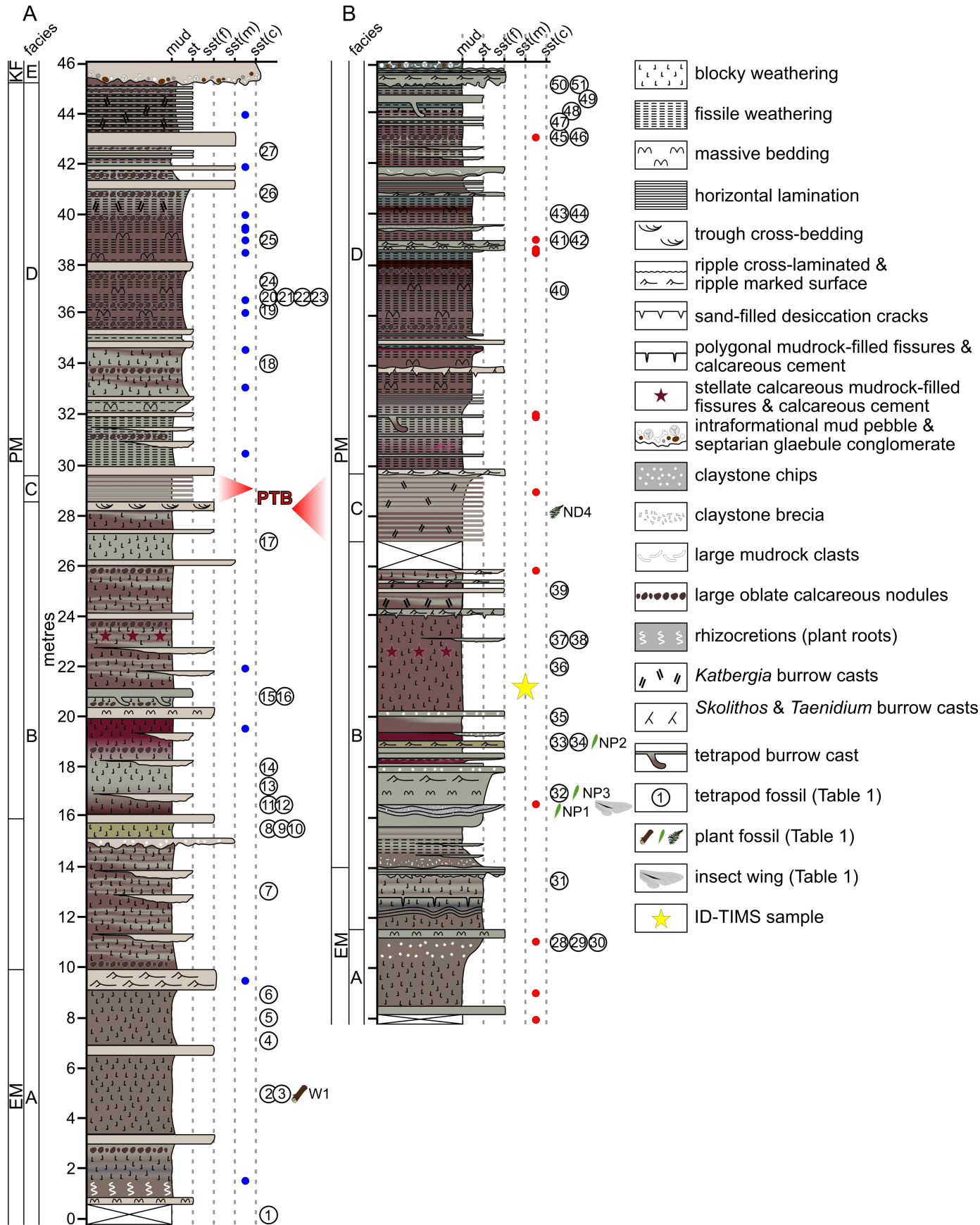


Figure 3

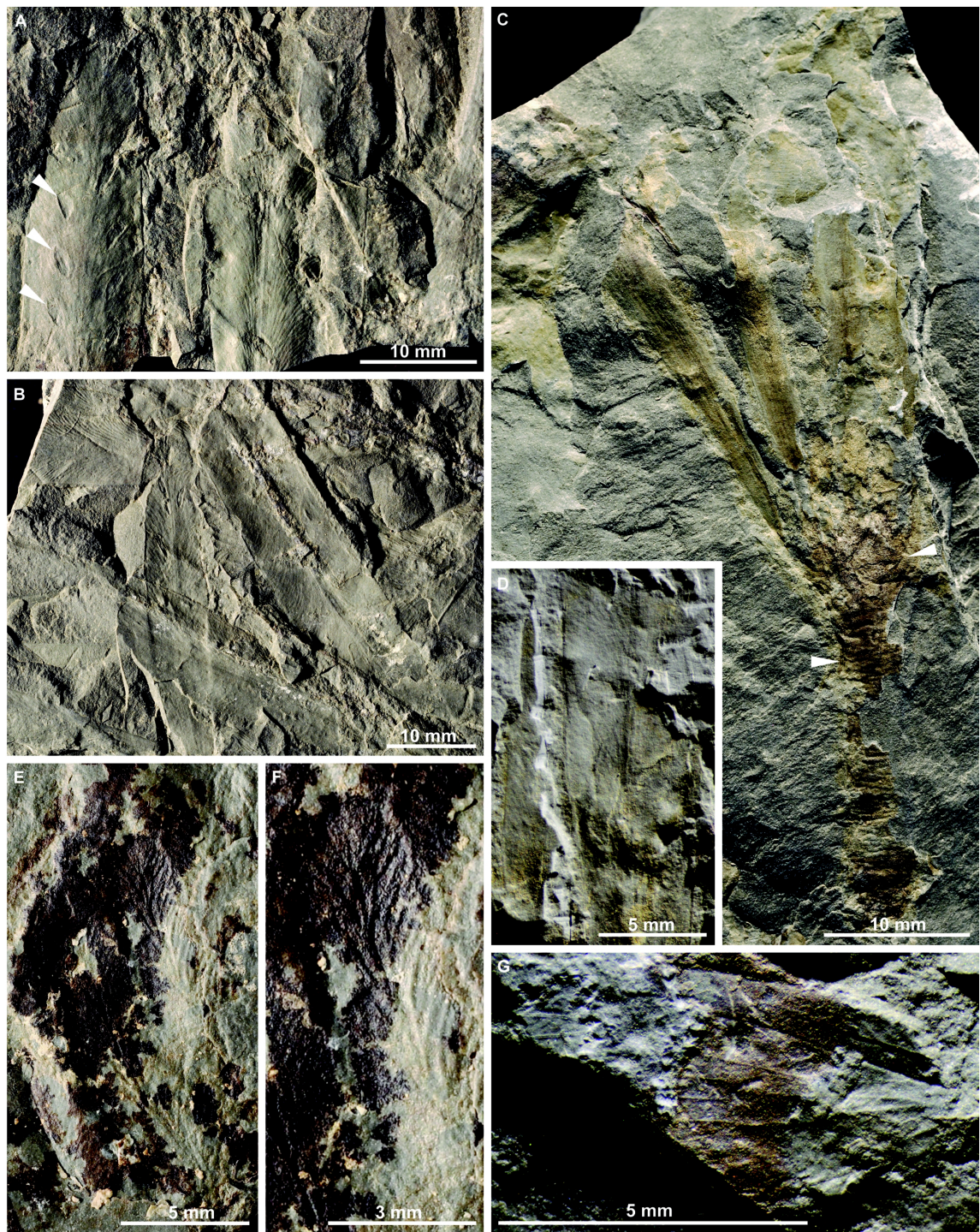


Figure 4

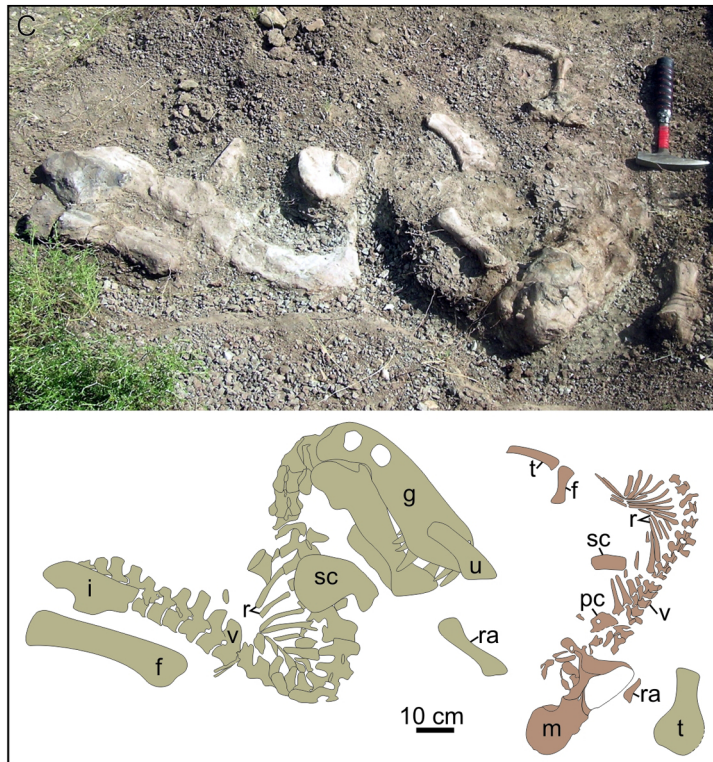
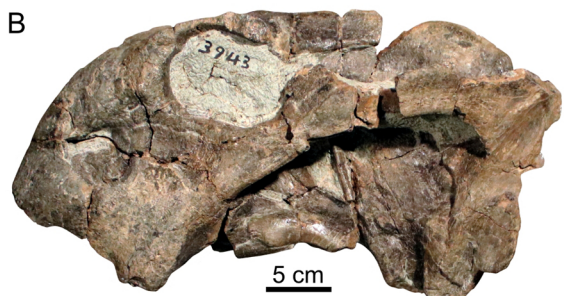
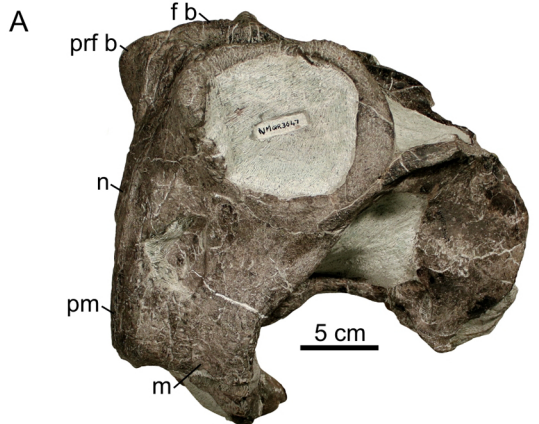


Figure 5



Figure 6

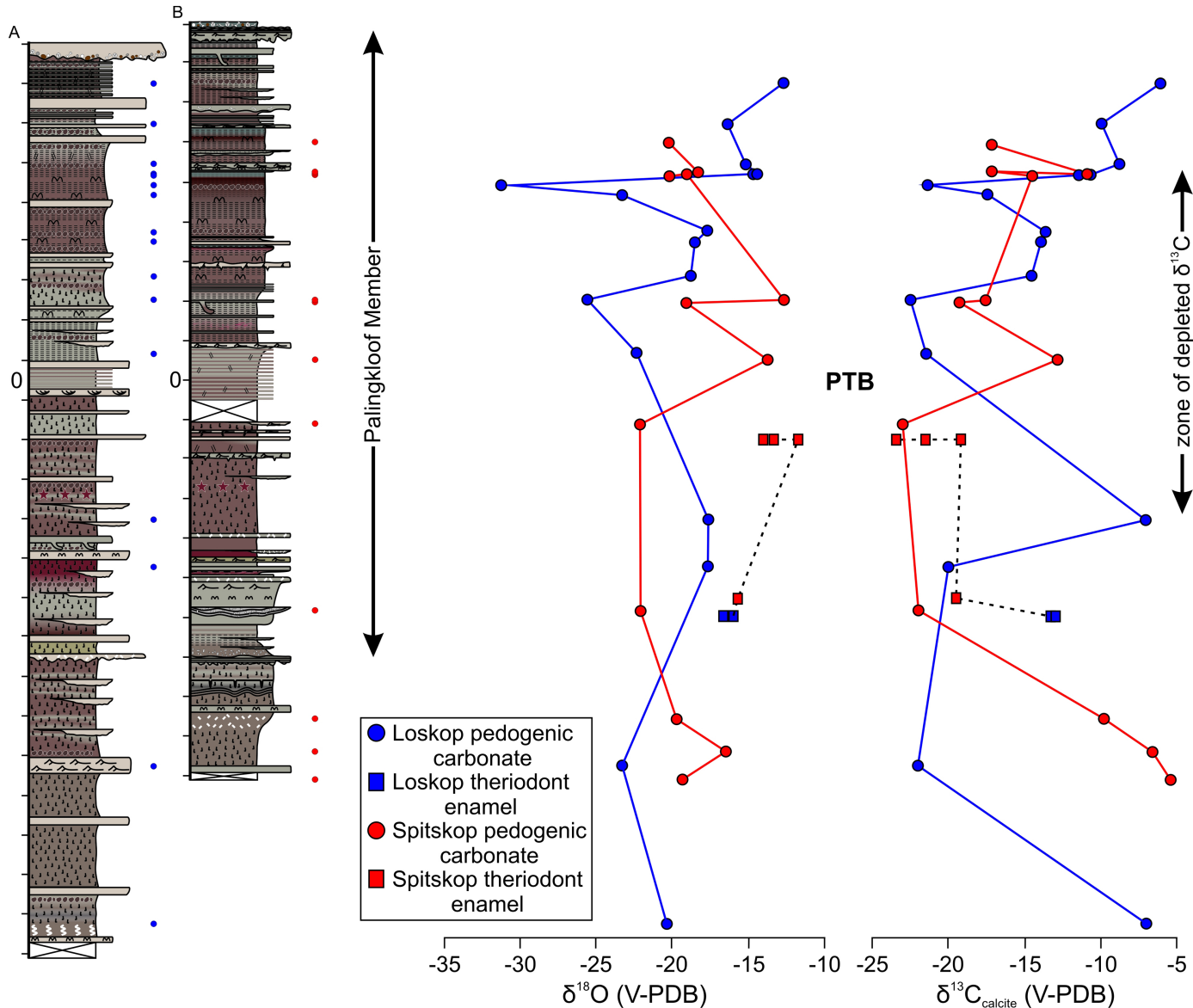


Figure 7

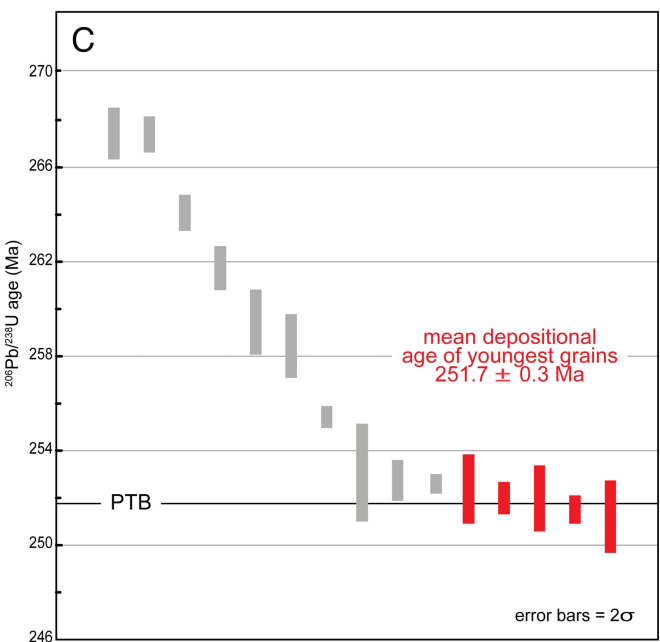
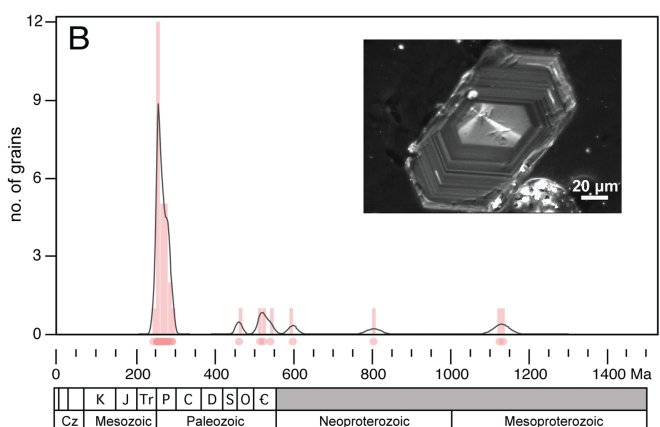
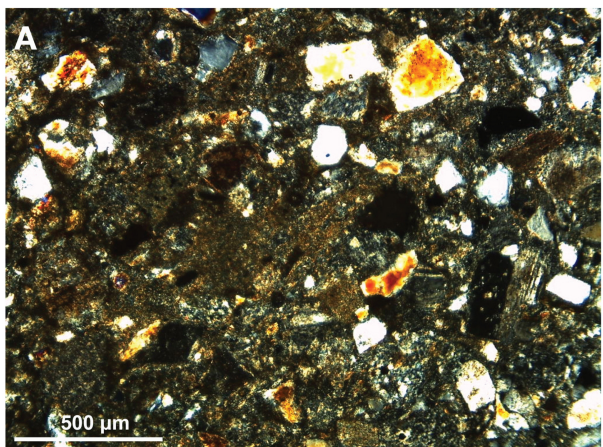


Figure 8

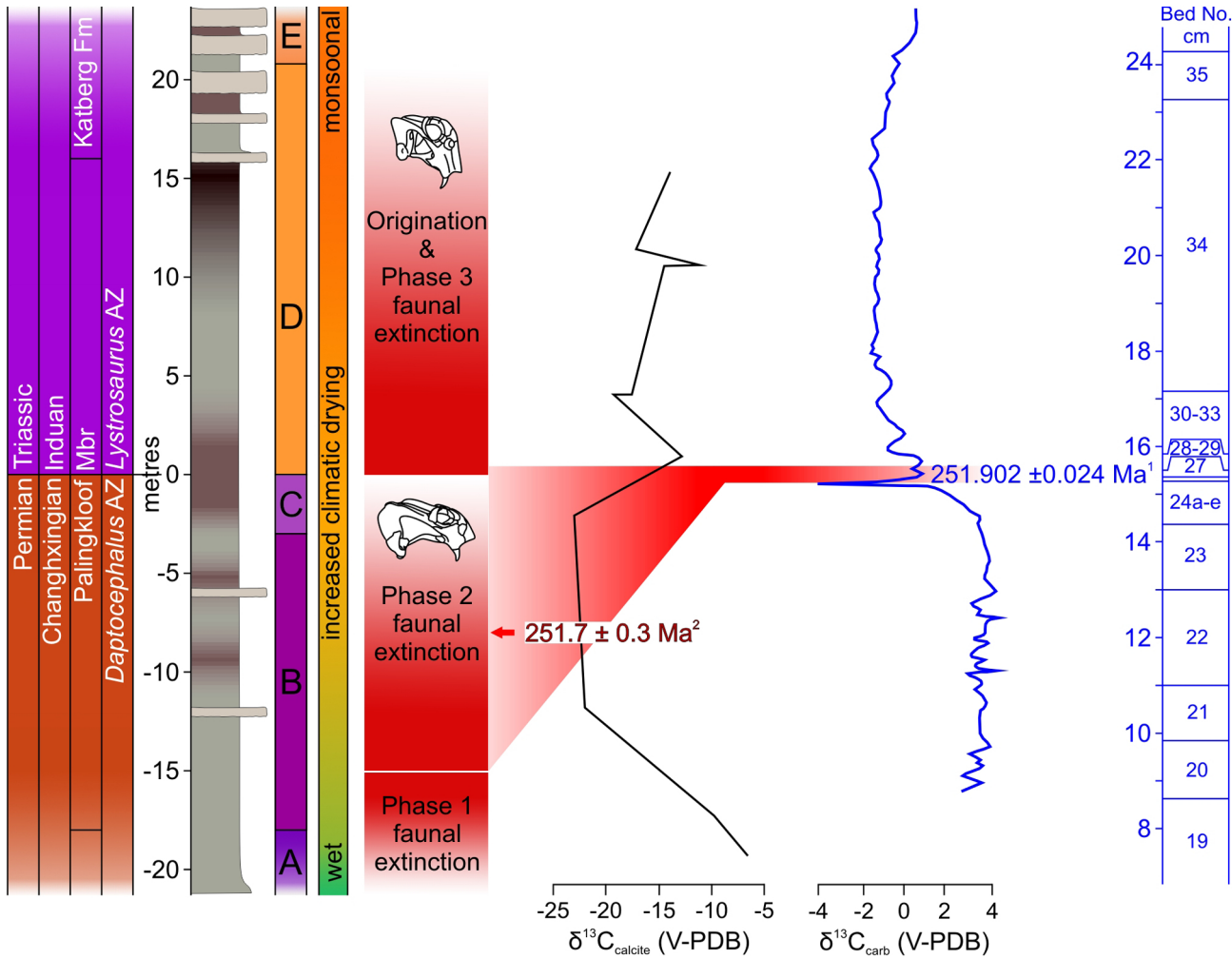


Figure 9

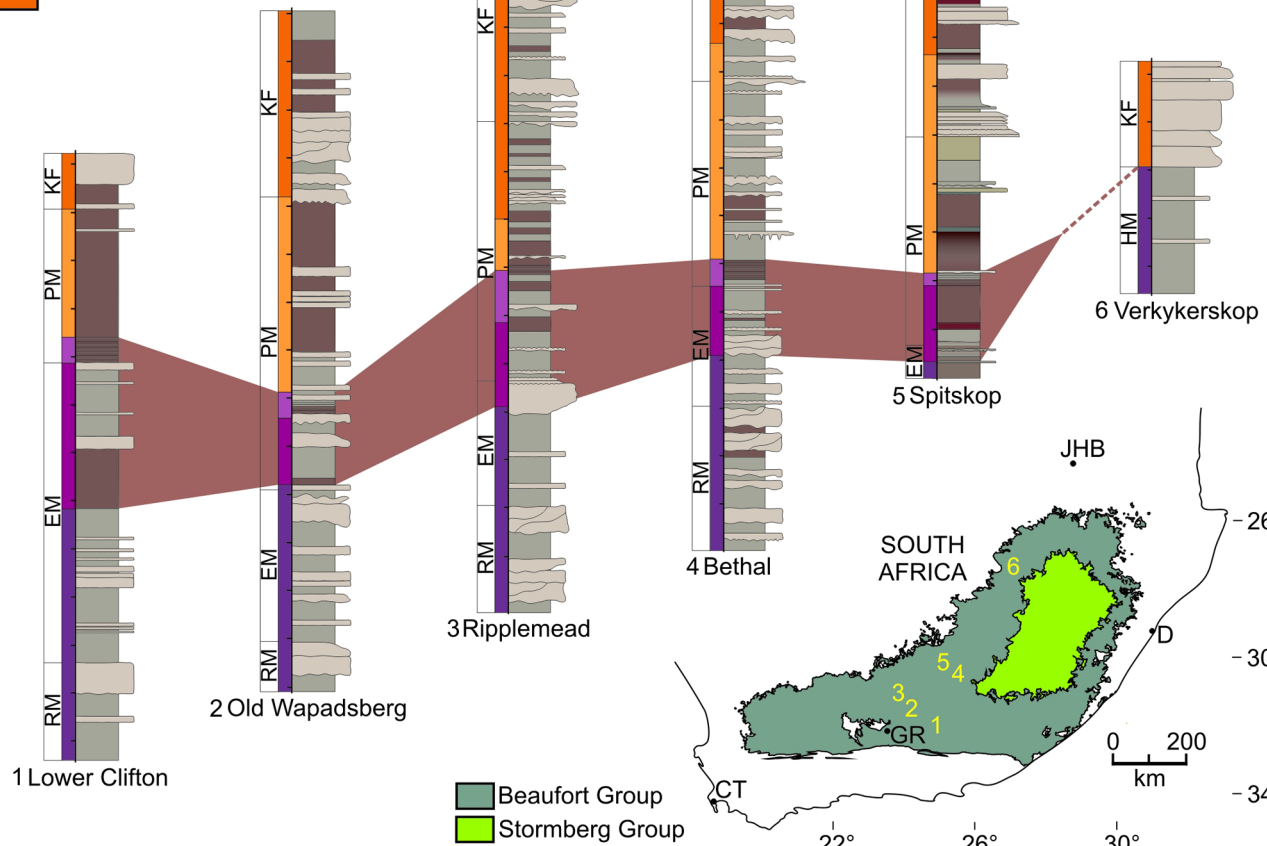


Figure 10